Incipient axial collapse of the Main Cordillera and strain partitioning gradient between the central and Patagonian Andes, Lago Laja, Chile

Daniel Melnick,[1,2] François Charlet,[3] Helmut P. Echtler,[1] and Marc De Batist[3]

Received 25 October 2005; revised 4 June 2006; accepted 3 August 2006; published 4 October 2006.

[1] Lago Laja is a late Quaternary volcanic-dammed lake located near the drainage divide of the south central Andes. Field observations, lake reflection seismic profiles, bathymetry, and remote sensing data reveal an active fault system that runs parallel to the volcanic arc along the axis of the Main Cordillera, the Lago Laja fault system (LLFS). Normal faults of this extensional system cut late Pleistocene volcanics, <7.1 ka still water lacustrine sediments, 6.3 ka pyroclastic deposits, and Holocene alluvial fans. We divide the LLFS in three segments on the basis of fault geometry, width, and slip magnitude. The underwater faults of the central segment in the lake's deepest part have the maximum Holocene vertical slip rate of >2.7 mm/yr. Since 7.1 ka, the LLFS accounts for ~0.7% of arc-normal extension at an average minimum rate of 1.2 mm/yr and strain rate of $\sim 10^{-14}$ s^{-1}. Seismites and surface ruptures evidence M>6 paleoearthquakes. The Main Cordillera at ~37°S is a large-scale pop-up structure uplifted by thrusting along its foothills. In this light, we interpret extension in the axial and highest part of the Andes as incipient synorogenic gravitational collapse in response to uplift and crustal thickening. Thermal weakening due to elevated heat flow and postglacial lithospheric rebound and unbending have probably contributed to the arc-limited collapse and Holocene acceleration of deformation rates. The lack of significant strike-slip offsets along the LLFS as well as along both foothills-thrust systems at 37°S contrasts with the intra-arc dextral fault zone south of 38°S. Regional structural data indicates that north of 38°S, diffusely distributed strain reflects low partitioning of oblique subduction, while to the south deformation is localized in a discrete strike-slip fault zone along the volcanic arc, reflecting a higher degree of partitioning. We relate this strain partitioning gradient to favorable fault orientations in the fore arc north of the Arauco Peninsula, a major seismotectonic boundary. **Citation:** Melnick, D., F. Charlet, H. P. Echtler, and M. De Batist (2006), Incipient axial collapse of the Main Cordillera and strain partitioning gradient between the central and Patagonian Andes, Lago Laja, Chile, *Tectonics*, *25*, TC5004, doi:10.1029/2005TC001918.

1. Introduction

[2] Continental margins usually deform over broad regions [e.g., *Molnar*, 1988], and in oblique plate convergent settings strain is frequently partitioned in a discrete strike-slip fault system and zones of diffuse deformation [e.g., *Fitch*, 1972; *Jarrard*, 1986; *Tikoff and Teyssier*, 1994; *Teyssier et al.*, 1995; *Avé Lallemant and Oldow*, 2000]. Mountain belts result from crustal shortening and thickening, but depending on its evolutionary state and on the physical properties of the lithosphere, strain may be partitioned into contraction along the mountain's foothills and coeval extension or transtension along its axis [e.g., *Dalmayrac and Molnar*, 1981; *Mercier et al.*, 1987; *Molnar and Lyon-Caen*, 1988; *Buck and Sokoutis*, 1994; *Royden*, 1996; *Liu et al.*, 2000].

[3] Active strain partitioning occurs at crustal scale along the Andean subduction margin [e.g., *Dewey and Lamb*, 1992; *Siame et al.*, 2005], but although plate convergence is constant along the margin [*Somoza*, 1998; *Kendrick et al.*, 2003], the degree of partitioning and consequent structural styles, and distribution of strain magnitude and seismic moment release vary markedly along strike. Major along-strike segmentation of the Andes has been correlated with changes in dip and age of the subducting plate, as well as with the presence of oceanic ridges and inherited continental discontinuities [e.g., *Jordan et al.*, 1983; *Mpodozis and Ramos*, 1989; *Ramos*, 1999; *Yáñez and Cembrano*, 2004]. However, the detailed structure of some transitional zones and their control on the seismotectonic segmentation of the margin remain poorly understood.

[4] A high degree of partitioning characterize the Patagonian Andes (38–46°S), where most of the margin-parallel component of oblique convergence has been accommodated by a strike-slip fault zone along the volcanic arc (Figure 1) [*Lavenu and Cembrano*, 1999; *Rosenau et al.*, 2006]. The margin-normal component is absorbed by the subduction interface and crustal faults in the coastal region as no thrusting has occurred in the foreland since late Miocene time [*Giacosa and Heredia*, 2004; *Melnick et al.*, 2006a].

[1] GeoForschungsZentrum Potsdam, Potsdam, Germany.
[2] Institut für Geowissenschaften, Universität Potsdam, Potsdam, Germany.
[3] Renard Centre of Marine Geology, University of Ghent, Ghent, Belgium.

0278-7407/06/2005TC001918

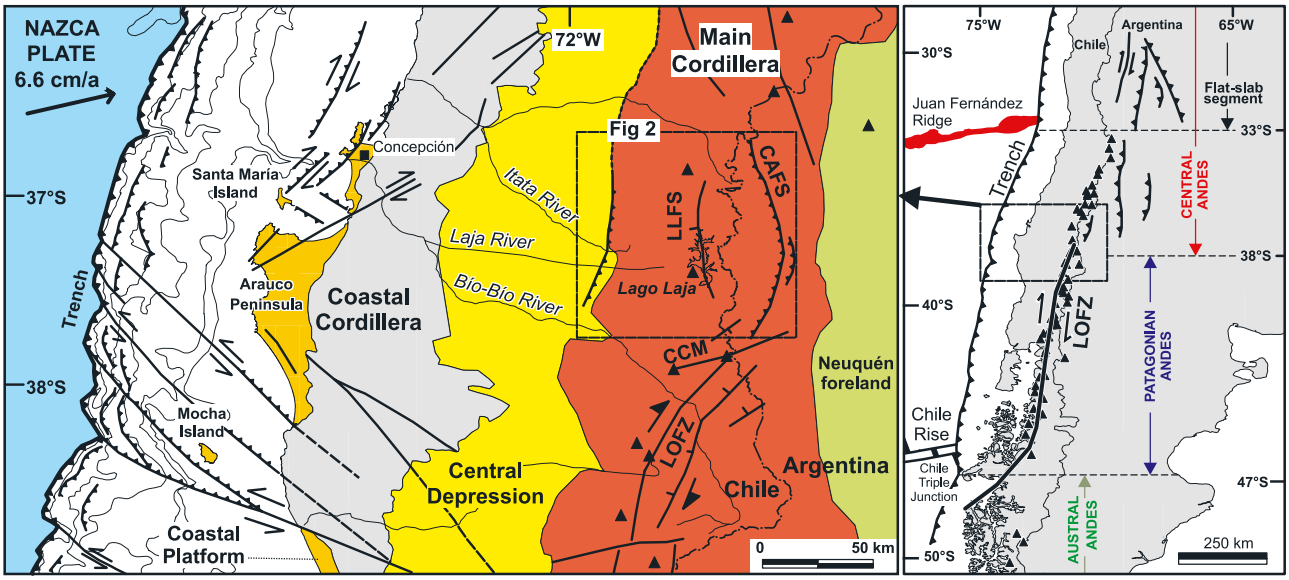

Figure 1. (right) Location map with main neotectonic structures and Andean segments [*Mpodozis and Ramos*, 1989; *Folguera et al.*, 2002]. LOFZ, Liquiñe-Ofqui fault zone. Flat slab foreland structures are from *Siame et al.* [2005]. Triangles denote Holocene volcanoes. (left) Regional morphotectonic units and Plio-Quaternary faults of the study region. LLFS, Lago Laja fault system; CAFS, Copahue-Antiñir fault system; CCM, Callaqui-Copahue-Mandolegüe. The offshore and coastal structures have been interpreted from multibeam bathymetry acquired by *Reichert and the SPOC Team* [2002], crustal seismicity, focal mechanisms, and industry reflection seismic profiles [*Melnick et al.*, 2006b; *Melnick and Echtler*, 2006].

The Patagonian intra-arc region has relatively low crustal seismicity and only two studies have reported focal mechanisms from shallow earthquakes that can be related to the geometry and kinematics of a surface fault [*Chinn and Isacks*, 1983; *Barrientos and Acevedo-Aranguiz*, 1992]. In contrast, along the flat slab segment of the central Andes (33–28°S) abundant shallow seismicity and Pliocene to Recent deformation has occurred mainly in the foreland region, partitioned into wide thrust belts and subordinated zones of strike-slip faulting [*Siame et al.*, 2005]. The transitional region (33–38°S) between the flat slab and Patagonian segments lacks previous detailed neotectonic studies, although three shallow M>7 earthquakes related to upper crustal faults of the intra-arc region are described in the <500 year historical record [*Lomnitz*, 2004]; no causative structures have been proposed yet and virtually nothing is known about seismogenic faults in this part of the high Andes. Between 33 and 34°S, superficial microearthquake clusters have been tentatively related to mapped faults or lineaments [*Barrientos et al.*, 2004], still, their paleoseismicity and relation to the historical M>7 events remain unexplored. Many lakes exist in this region of the high Andes, most are of glacial or volcanic origin while others result from natural damming by landslides or volcanic deposits, and from artificial barriers made for hydropower generation, irrigation, or to store mining residue. Since these lakes are in a seismically and volcanically active region, where related processes could lead to the sudden opening of a lake's dam, the generation of outburst megafloods along the steep western flank of the Andes pose one of the highest hazards to settlements in the foothills, the Central Depression, and even the coastal region. Wide fans with volcanic boulders spread in the flat Central Depression are testimonies of past catastrophic outburst floods [e.g., *Thiele et al.*, 1998].

[5] We focus on the southernmost central Andes, where most of the studied active deformation has been east vergent thrusting in the back-arc and foreland regions. The aim of this study is mainly to document an active extensional fault system adjacent to a volcanic-dammed lake in the higher part of the Main Cordillera, the Lago Laja fault system. We describe the kinematics, deformation rates, and earthquake hazards of this fault system by integrating field observations with offshore-lake seismic profiles, bathymetry, and remote sensing images. Soft-sediment deformation structures affecting late Pleistocene glaciolacustrine deposits adjacent to the fault system are discussed as indicators of paleoseismicity. Furthermore, we document Quaternary folding in response to shortening locally along the western foothills of the Main Cordillera and integrate regional neotectonic data in an arc-normal profile. In this light, the extensional deformation along the Main Cordillera's axis is interpreted as caused by incipient gravitational collapse in response to coeval shortening along both its eastern and western foothills. Active structures in the fore-arc and intra-arc regions are integrated to propose a transition zone in the degree of strain partitioning and to discuss the causes and resulting

changes of the distribution of active deformation, structural styles, and topography along the margin.

2. Methods

[6] Active faulting along the Lago Laja fault system is documented through field geologic, geomorphic, and structural mapping, interpretation of rectified aerial photos and satellite imagery. Digital elevation models (DEM) made from digitized 1:50,000 topographic maps, SRTM-NASA data, and photogrammetric restitutions of 1:70,000 scale aerial photos aided in the identification and mapping of landforms and active structures. Published isotopic ages from the youngest deposits cut by the fault system were compiled to estimate deformation rates. Radiocarbon ages were calibrated using the CalPal 2005 software (http://www.calpal.de) [*Stuiver et al.*, 1998; *Hughen et al.*, 2004]. Within the framework of paleoclimatic and limnologic research, high-resolution reflection seismic data were collected at Lago Laja by the Renard Center for Marine Geology, University of Ghent, Belgium (RCMG) [*Charlet et al.*, 2003]. They were recorded using a "Centipede" multielectrode sparker, which operated at 500 J with a signal frequency range of 100–1500 Hz, and a subbottom profiler (Transducer MountModel 132B, 3.5 kHz) composed of a transmitter Model 5430A and a receiver Model 5210A. A total of 72 km of reflection lines were shot, 25 km sparker and 47 km pinger (3.5 kHz). The subaqueous faults of Lago Laja were mapped from selected 3.5 kHz profiles using the software package KINGDOM® at RCMG. In this cooperation, bathymetric profiles were collected by the UmweltForschungsZentrum Leipzig-Halle, Germany (UFZ), using a two-frequency echo sounder system (Simrad EA400) and a differential GPS. About 160 cross profiles were measured covering 350 km of track lines. The data was linearly interpolated to produce a DEM. To quantify fault throw, individual bathymetric profiles were correlated with the structures interpreted from the seismic lines.

3. Regional Tectonic and Geologic Setting

[7] The Andean margin is formed by subduction of the Nazca oceanic plate under the South American continent (Figure 1); this collision is responsible for the growth of the Andean orogeny over the last ~200 Myr [e.g., *Mpodozis and Ramos*, 1989]. The subducting Nazca plate at 37°S is formed by ~32 Ma oceanic crust [*Tebbens and Cande*, 1997], which converges at 80 mm/yr averaged over the last ~3 Myr [*Somoza*, 1998], or 66 mm/yr determined on the base of GPS modeling [*Kendrick et al.*, 2003].

[8] The Andes at ~37°S are subdivided in five major morphotectonic units (Figure 1): (1) the Coastal Platform, which consists of uplifted Cenozoic coastal sequences; (2) the Coastal Cordillera that integrates a late Paleozoic accretionary complex and magmatic arc; (3) the Central Depression, a low-relief area formed by Oligo-Miocene sedimentary and volcanic rocks covered by Plio-Quaternary sediments; (4) the Main Cordillera, focus area of this paper, consists of a long-lived Meso-Cenozoic magmatic arc and intra-arc volcano-sedimentary basins; and (5) the Neuquén Mesozoic embayment and late Cretaceous-Miocene foreland basin. Crustal thickness below the Main Cordillera is between 40 and 45 km in the 37–39°S region, as estimated from refraction seismic profiles [*Lüth et al.*, 2003], P wave tomography [*Bohm et al.*, 2002], receiver functions [*Yuan et al.*, 2006], and gravity modeling [*Tassara et al.*, 2006].

[9] Between 36 and 39°S, the Main Cordillera integrates the late Oligocene–middle Miocene Cura-Mallín and Trapa-Trapa formations [*Niemeyer and Muñoz*, 1983], which have been interpreted as the infill of the Cura-Mallín extensional intra-arc basin [*Jordan et al.*, 2001; *Kemnitz et al.*, 2005]. The Main Cordillera was uplifted during the late Miocene through inversion of the Cura-Mallín basin [*Jordan et al.*, 2001; *Melnick et al.*, 2006a]. Orogenic shortening formed a mountain belt about 2 to 2.5 km high and 80 km wide. This mountain building phase is recorded along most of the central and southern Andes and has a diachronic evolution and marked along-strike variations in shortening magnitude and deformation style [e.g., *Kley et al.*, 1999]. Between 38 and 39°S, shortening in the intra-arc started at ~11 Ma and stopped before 5.6 Ma, as shown by ages of the synorogenic and oldest posttectonic deposits, respectively [*Melnick et al.*, 2006a]. Plateau volcanic rocks, referred to as the Cola de Zorro Formation of Pliocene–early Pleistocene in age [*Vergara and Muñoz*, 1982], overlay the former units in a marked angular unconformity (Figure 2).

[10] At 37°S in the coastal region, shallow crustal seismicity registered by a temporary network [*Bohm et al.*, 2002], focal mechanisms [*Bruhn*, 2003], and industry reflection seismic profiles show that dextral oblique shortening is occurring along northeast striking reverse faults, which extend from Isla Santa María to the northeast (Figure 1) [*Melnick et al.*, 2006b]. In contrast, south of the Arauco Peninsula, the same data sets image similar active faults, which in turn strike northwest and accommodate left-lateral oblique shortening. Therefore two coastal kinematic domains exist, the domain south of Arauco where active faults strike northwest and have a left-lateral component, and the domain to the north where in turn active faults strike northeast and have a right-lateral component (Figure 1). Seismic stratigraphy of syntectonic deposits correlated with ENAP hydrocarbon exploration boreholes indicate that these structures have been continuously active since the late Pliocene with constant kinematics [*Melnick et al.*, 2006b; *Melnick and Echtler*, 2006].

[11] After the southeast Pacific plates reorganization at ~10 Ma [*Tebbens and Cande*, 1997], convergence obliquity along the Andean margin increased continuously south of ~20°S, inducing strain partitioning along the margin [e.g., *Dewey and Lamb*, 1992]. No Pliocene-Quaternary foreland fold-and-thrust belt has been recognized in the Patagonian Andes (38–47°S), where about half of the margin-parallel component of oblique subduction has been accommodated along the intra-arc region by the strike-slip Liquiñe-Ofqui fault zone (LOFZ in Figure 1) [*Rosenau et al.*, 2006]. The LOFZ is a ~1200-km-long dextral system that extends

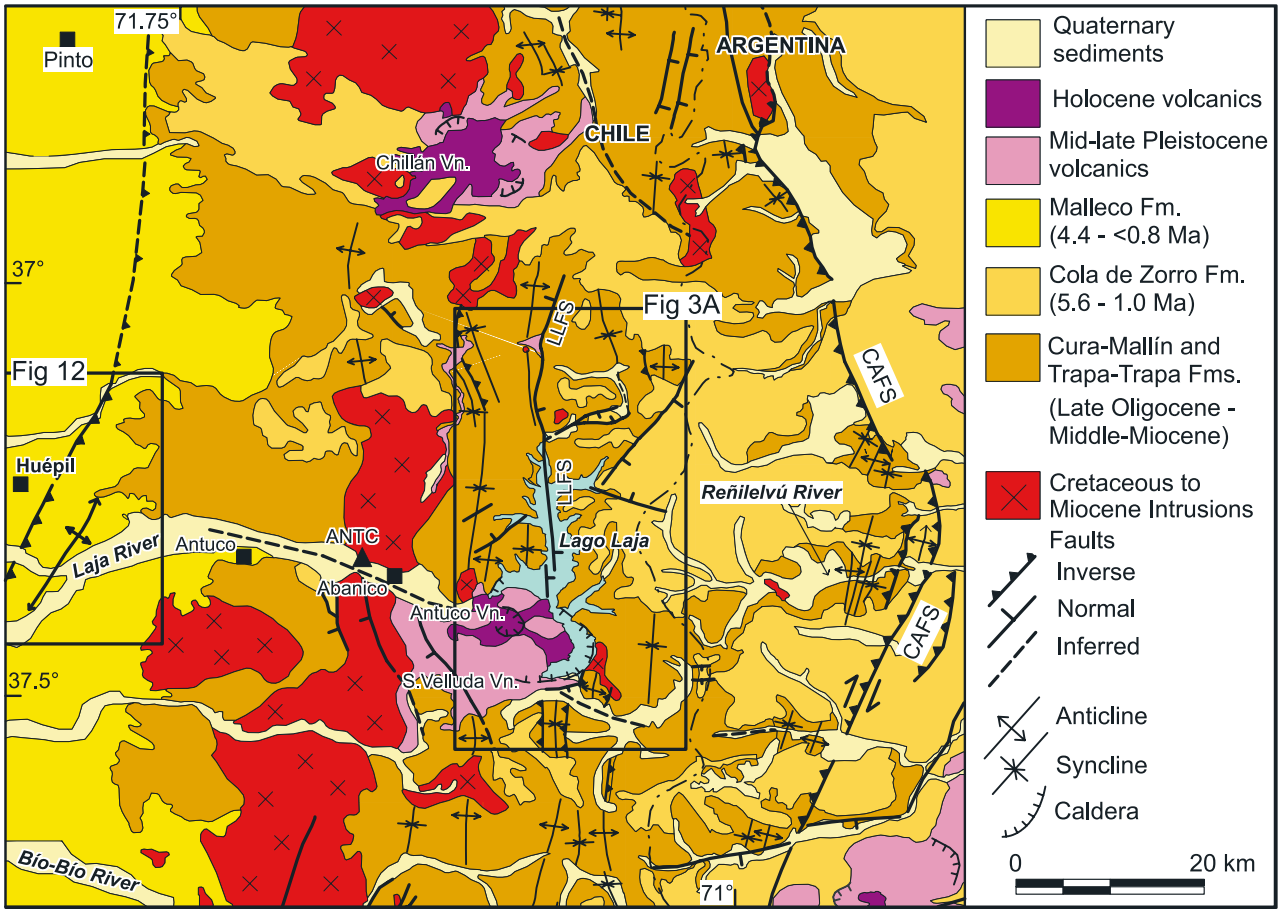

Figure 2. Regional geologic map of the Main Cordillera. LLFS, Lago Laja fault system; CATF, Copahue-Antiñir thrust front. Compiled from *Niemeyer and Muñoz* [1983], *Delpino and Deza* [1995], *Folguera et al.* [2004], *Melnick et al.* [2006b], and new field observations.

from 47°S, immediately south of the Chile Triple Junction, until 38°S [e.g., *Cembrano et al.*, 1996; *Lavenu and Cembrano*, 1999]. At its northern end, the Callaqui-Copahue-Mandolegüe crustal-scale transfer zone (Callaqui-Copahue-Mandolegüe (CCM) in Figure 1) [*Melnick et al.*, 2006a] decouples the LOFZ-related strike-slip deformation from the Copahue-Antiñir contractional back-arc system and the Lago Laja extensional intra-arc system, the focus of this paper.

4. Study Area: Lago Laja

[12] Lago Laja, also known as Laguna de la Laja, is a narrow volcanic-dammed lake located along the axis of the volcanic arc (Figures 1 and 2). The lake has a surface of 95 km^2 and a watershed area of 975 km^2. The maximum length and width are 32 and 9 km, respectively, and the total shoreline length is 136 km. The lake is formed by three connected subbasins, two shallow parts in the south and north, and a central deeper part (Figure 3). At a water level of 1346 m, the maximum depth is 134 m and the estimated volume is 4.7 km^3. The lake is fed by several small streams, torrential rivers, and the meandering Pinos River on the southern part, and is drained by the Laja River and two artificial tunnels made for hydropower generation. Mean annual precipitation is 2170 mm/yr, mostly as snow during the winter (Dirección Meteorológica de Chile, 2005, http://www.meteochile.cl). Many strandlines are present along the shore due to the large fluctuations of the water level. Annual variations in lake level have reached 60 m, causing volume changes of up to 3 km^3, due to management by hydroelectric power stations during dry years [*Bevis et al.*, 2004].

4.1. Origin of Lago Laja

[13] The 2979-m-high Antuco and 3585-m-high Sierra Velluda stratovolcanoes are located on the southwestern border of Lago Laja (Figures 2 and 3a). Both are Quaternary edifices with ages at the base of <124 and 495 ± 88 ka, respectively (K-Ar/whole rock [*Moreno et al.*, 1985]). The Sierra Velluda is inactive and deeply eroded by glaciations, while the Antuco erupted at least 19 times since 1624, latest in 1911 [*Petit-Breuilh*, 1994]. In contrast to most of the stratovolcanoes in the southern Andes, the base of these edifices is topographically lower than their surrounding Tertiary basement. Both volcanoes are emplaced in the western part of an ~18-km-diameter annular depression

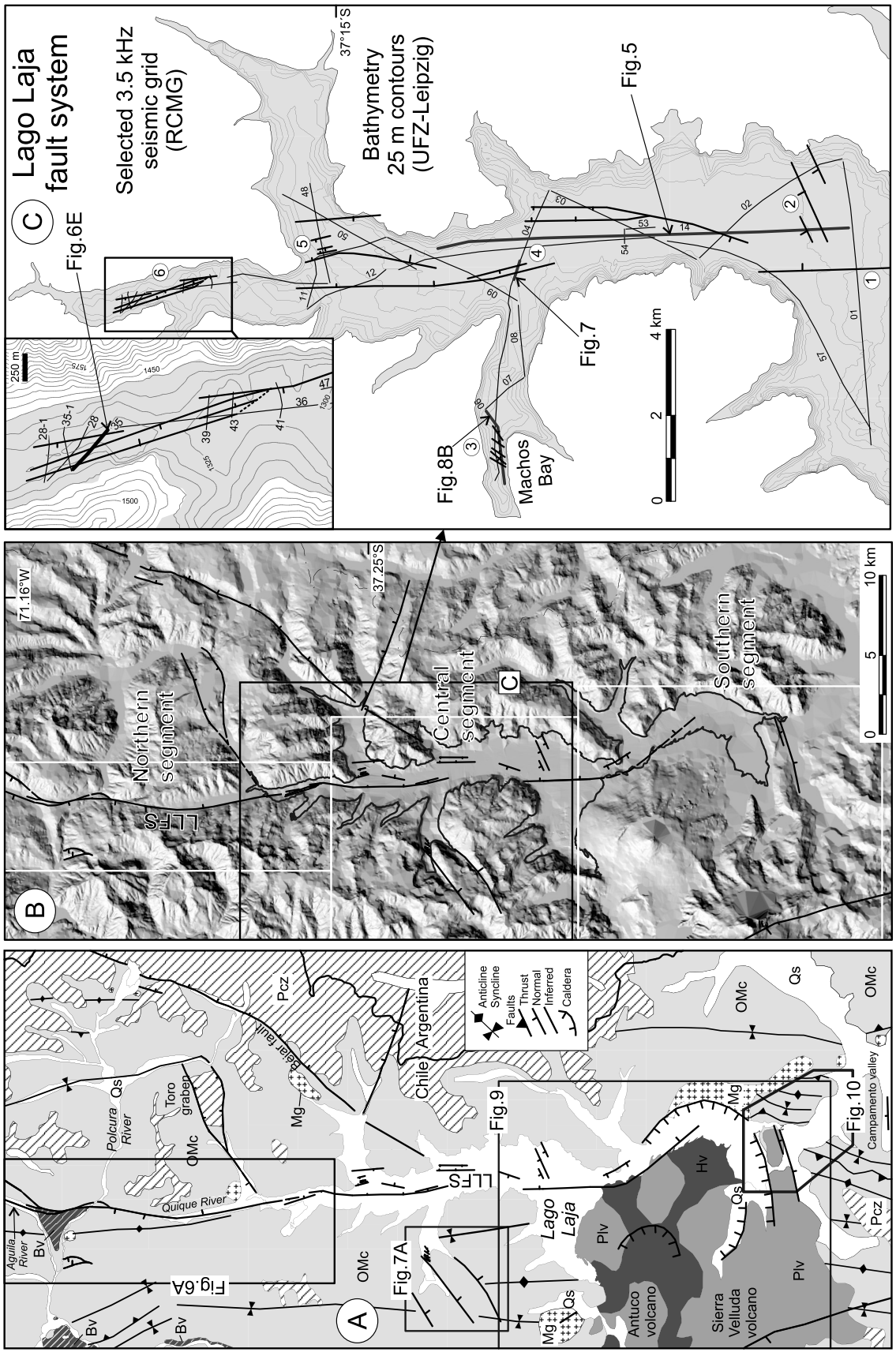
A
B
C
Lago Laja fault system
Selected 3.5 kHz seismic grid (RCMG)
Bathymetry 25 m contours (UFZ-Leipzig)
Fig.6E
Fig.5
Fig.7
Fig.8B
Machos Bay
37°15'S
71.16°W
37.25°S
LLFS
Northern segment
Central segment
Southern segment
Chile
Argentina
Baker fault
Toro graben
Polcura River
Quique River
Agulia River
Campamento valley
Lago Laja
Antuco volcano
Sierra Velluda volcano
Fig.6A
Fig.7A
Fig.9
Fig.10
Anticline
Syncline
Faults
Thrust
Normal
Inferred
Caldera
Bv
Qs
OMc
Mg
Pcz
Plv
Hv
0
2
4 km
5
10 km
250 m

Figure 3

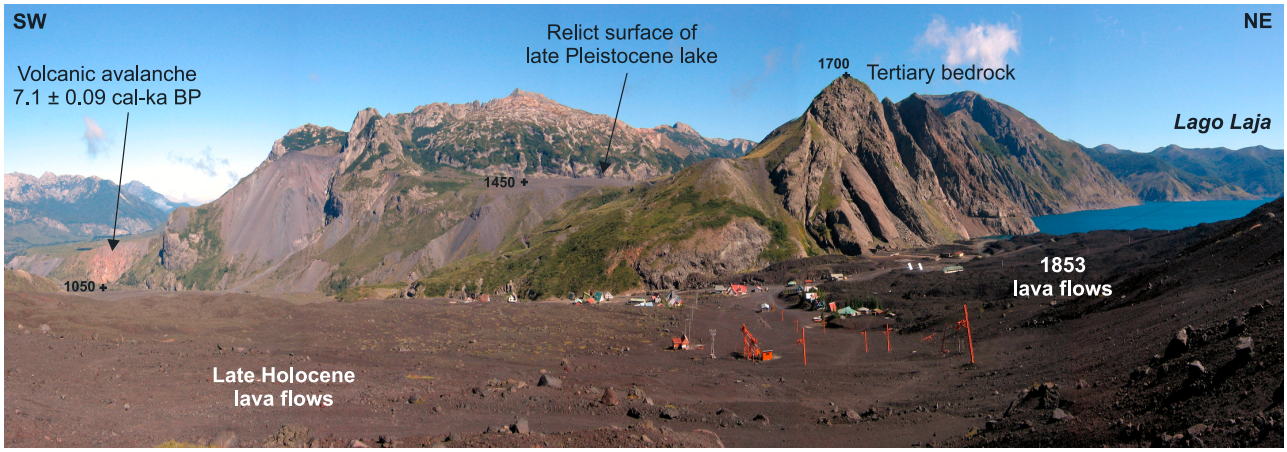

Figure 4. Panoramic view from the foothills of the Antuco volcano toward the northwest (see Figure 9 for location). The Holocene volcanic avalanche can be seen on the lower left. Calibrated radiocarbon age is from *Lohmar* [2000]. The late Holocene lava flows on the lower part conform the dam of the present lake. The darker flows on the lower right were emitted during the 1853 eruption and dammed the outlet of Lago Laja causing its waters to rise about 20 m [*Petit-Breuilh*, 1994]. In the central part a relict late Pleistocene lacustrine surface is seen. Crosses indicate reference elevations in meters.

(Figures 2 and 3a), where they dam the drainage network forming the Laja intramontane basin.

[14] The Antuco volcano evolved in two stages: Antuco 1, started erupting at ~130 ka with the building of the basaltic-andesitic edifice and culminated with a Bandai-type caldera collapse event; and during the ongoing Antuco 2 stage a 500-m-high cone formed in the center of the cuspidate caldera created at the end of the previous stage, as well as six flank vents and cinder cones [*Domeyko*, 1846; *Brüggen*, 1941; *Vergara and Katsui*, 1969; *Moreno et al.*, 1985, 2000; *Thiele et al.*, 1998; *Lohmar*, 2000] (Figure 3a). The volcanic avalanche ejected at the end of the first stage caused the opening of Lago Laja's dam generating an outburst megaflood [*Vergara and Katsui*, 1969; *Thiele et al.*, 1998]. Subsequent lava flows emitted during the second stage dammed the Laja River forming the present-day Lago Laja. Two radiocarbon ages have been reported for this volcanic avalanche: 9.70 ± 0.6 [*Moreno et al.*, 1985] and 6.25 ± 0.06 ka [*Lohmar*, 2000]. We favor the latter age because the analytic error is much lower. This age was obtained from a large piece of *Nothofagus dombeyi* found 2 km northwest of Abanico (Figure 2) inside a hummock of the volcanic avalanche; it has a calibrated value of 7.143 ± 0.09 cal ka (calibrated thousand years before present). The lava flows emitted during the Antuco's last major eruption in 1852–1853 (Figure 4) covered the outlet of Lago Laja causing the waters to rise ~20 m [*Petit-Breuilh*, 1994].

4.2. Lake Stratigraphy From Reflection Seismic Profiles

[15] The sparker and pinger (3.5 kHz) data show a complex seismic stratigraphy with limited penetration. The profiles indicate a strong influence in the southern part of the lake by volcanic input from the Antuco. Several units, which could correspond to successive volcanic events, are thinning out northward away from the volcano. Fluid escape features and free-gas pockets are observed locally. In the central and northern sectors, a lacustrine drape overlies these volcanic lacustrine units above an erosive unconformity (Figure 5). This drape is formed by continuous parallel reflectors, typical of Holocene lacustrine sediments in glaciated environments [e.g., *Eyles et al.*, 2000]. This acoustically laminated seismic facies, however, without confirmation from sediment cores, suggests that the sediments are typical still water lacustrine deposits, composed of laminations formed by suspension settling, similar to the sediments recovered in other lakes in the region [e.g., *Bertrand et al.*, 2005]. The lacustrine drape has a fairly uniform thickness of 2 to 3 ms TWT (two-way traveltime), about 1.6 to 2.4 m. We relate this erosional surface to the Holocene caldera-collapse event at the end of the Antuco 1 stage, which caused the opening of Lago Laja generating an outburst megaflood. The lake was probably emptied during this event because the >150-m-high present-day dam, which is exclusively formed by postcollapse lava flows (Figure 4), is higher than the maximum depth of the lake. Therefore after the opening of the dam the fluvial

Figure 3. (a) Geologic map of Lago Laja region, modified from *Niemeyer and Muñoz* [1983] and *Melnick et al.* [2006a]. Geologic units are OMc, Cura-Mallín and Trapa-Trapa formations (Oligocene–middle Miocene); Mg, intrusives (late Miocene); Pcz, Cola de Zorro Formation (Pliocene–early Pleistocene); Plv, middle–late Pleistocene volcanics; Bv, late Pleistocene valley-confined basalts; Hv, Holocene volcanics; Qs, Quaternary sediments. (b) Shaded relief DEM made from 1:50,000 topographic maps (50-m contours) and detailed bathymetric profiles. Quaternary extensional faults are shown. The white boxes indicate the three segments of the Lago Laja fault system discussed in the text. (c) Location of selected 3.5 kHz reflection seismic profiles and map of Holocene faults interpreted from these lines.

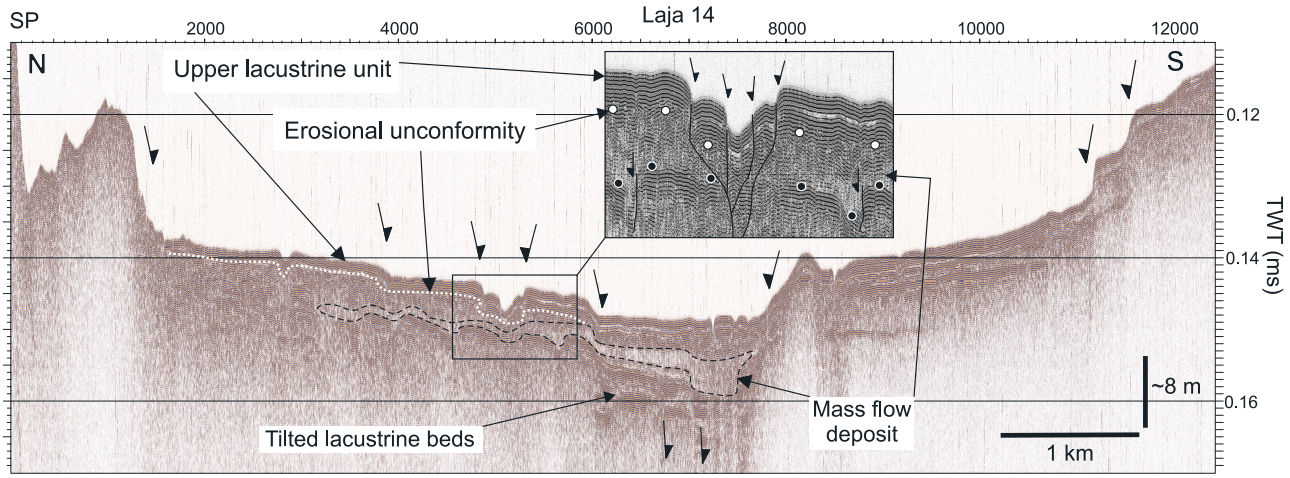

Figure 5. Reflection seismic profile Laja 14 (3.5 kHz) illustrating the stratigraphy and structure of the central part of Lago Laja. For location, see Figure 3c. SP, shotpoint; TWT, two-way traveltime. The upper lacustrine drape covers the older sequences in an erosional unconformity. We relate this erosional phase to the 7.1 ka Antuco 1 caldera collapse event, which broke Lago Laja's dam causing an outburst megaflood. The lake was totally emptied, and the fluvial systems advanced into the lacustrine basin eroding the unconsolidated sediments and forming the unconformity; see text for details.

systems that feed the lake advanced into the deeper parts of the basin eroding the poorly consolidated lacustrine sediments. This erosional surface is thus synchronous to the Antuco 1 caldera collapse event dated at 7.1 ± 0.09 cal ka [*Lohmar*, 2000]. This horizon is observed in most of the seismic profiles and is therefore an excellent marker for structural analysis. The Holocene sedimentation rate would be 0.2–0.3 mm/yr, which is consistently lower than the 0.7–0.9 mm/yr rate determined for Lago Puyehue at 40°S by coring [*Bertrand et al.*, 2005]. Puyehue is a glacial lake located at much lower elevation (185 m above sea level (asl)), with much higher watershed-to-lake area ratio and elevated mean annual precipitation and sediment supply, therefore a higher sedimentation rate than at Laja should be expected.

[16] In the central part of Lago Laja, homogeneous, nonreflective massive layers are locally interbedded in the lacustrine sequence (Figure 5). These discontinuous beds thin out rapidly and are thus interpreted as debris or mass flow deposits, based on similarities with other lake seismic surveys in mountain regions where they have been verified by coring [e.g., *Chapron et al.*, 1999; *Schnellmann et al.*, 2002]. These instantaneous deposits could have been triggered by earthquake-induced ground shaking or by abnormally high precipitation events. However, the mass flow deposit imaged on profile 14 (Figure 5) increases in thickness toward the main northwest dipping fault, and may have been related to an earthquake that caused slip on this fault.

5. Lago Laja Fault System

[17] The Lago Laja Fault System (LLFS) strikes north-south and extends for ~60 km along the bottom of Lago Laja, Quique and Aguila valleys (Figure 3a). During their regional survey, *Niemeyer and Muñoz* [1983] first mapped the fault along the Quique valley, but kinematics and age were not determined. Recent faulting along this system was first recognized in offshore seismic profiles. These faults offset the most recent sediments of the lake bottom (Figure 5), generating relief on the lake bed. During consecutive field investigations, faults cutting Holocene pyroclastic deposits and alluvial fans were found north and southeast of the lake, and merged with the interpretation of seismic profiles to define and map the fault system.

[18] We subdivide the LLFS in three segments (Figure 3b): (1) the northern segment, were faulting occurs along a relatively narrow, north-south striking zone with meter-scale slip magnitude; (2) the central segment, which consists of a ~7-km-wide north-south striking zone of faulting and also oblique structures, and where slip can reach 20 m on individual faults; and (3) the southern segment, which has a poorly defined fault geometry masked by the Antuco volcanics and integrates soft-sediment deformation structures interpreted as seismites. Slip magnitude decrease in the southern segment and the fault pattern becomes irregular. Evidence for recent extensional tectonics is documented from surface ruptures, fault-controlled volcanic eruptions, and seismic and bathymetric profiles for each segment.

5.1. Northern LLFS Segment

5.1.1. Surface Ruptures

[19] North of Lago Laja along the Quique valley (Figures 3a and 6a), Holocene surface ruptures can be traced as fairly continuous features on aerial photos. The main fault strikes north-south and forms a ~1.5-m-high east-down scarp that cuts alluvial fans along the western flank of the valley. The rupture area is covered by dense vegetation, which

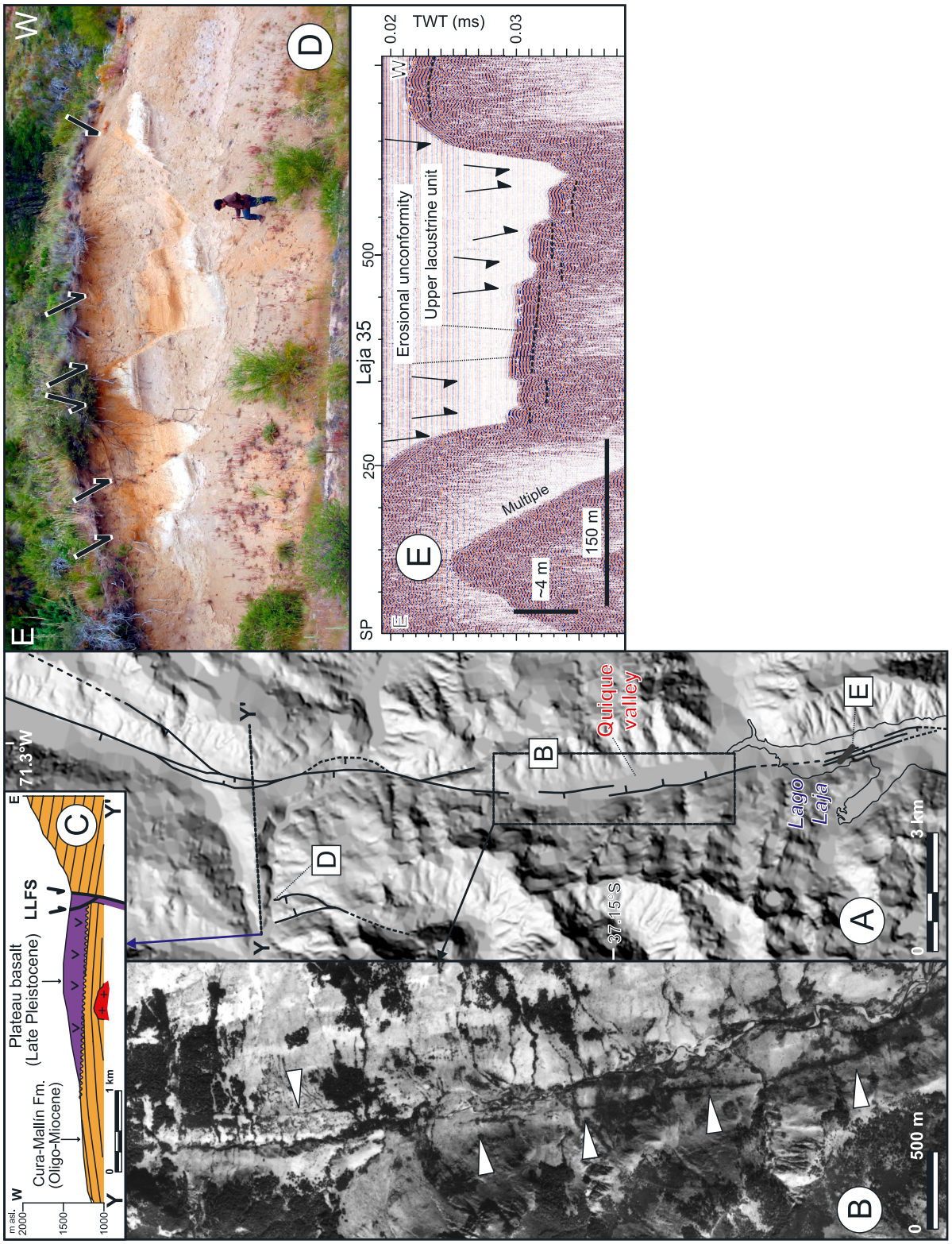
W
E
D
SP
Laja 35
500
250
TWT (ms)
0.02
0.03
Erosional unconformity
Upper lacustrine unit
Multiple
~4 m
150 m
E
C
Y
Y'
m asl.
2000
1500
1000
Plateau basalt
(Late Pleistocene)
Cura-Mallín Fm.
(Oligo-Miocene)
LLFS
1 km
71.3°W
37.15°S
Quique
valley
B
A
Lago
Laja
3 km
500 m

Figure 6

probably concentrates here due to waters springing through the densely fractured fault zone. The dense vegetation area is about 15–20 m wide and can be followed on the aerial photo for 3.5 km along the western flank of the valley, and northward for 1.5 km along the eastern flank (Figure 6b).

[20] Postglacial fallout pyroclastic deposits from the Chillán volcano, which is located ~25 km to the northwest (see Figure 2), cover most of the area north of Lago Laja. At a roadcut along the Polcura River, 10 north-south striking normal faults cut these pyroclastic deposits (Figure 6d). The faults form an asymmetric horst-and-graben structure with west-down polarity and 3.2 m slip on the main fault. *Dixon et al.* [1999] reported nine radiocarbon ages of pyroclastic deposits from the Chillán volcano, which range from 9.30 ± 0.07 to 2.27 ± 0.06 ka; calibrated values range from 10.46 ± 0.1 to 2.25 ± 0.07 cal ka. They subdivided these deposits based on their ages, facies, and spatial distribution in three groups: the ~10 ka basal sequence, the intermediate sequence that ranges from 6.1 to 6.5 cal ka, and the proximal deposits that have a ~2.2 cal ka age. Unfortunately, no datable material was found in the faulted pyroclastics of the Polcura River, but on the basis of their strong lithological and stratigraphical similarities and equivalent distance to the source, we correlate them with Dixon's intermediate group, which has a pooled age of 6.3 ± 0.2 ka. Assuming this age range, a slip rate of 0.50 ± 0.02 mm/yr is derived for the main west dipping fault.

[21] At the crossing of the Aguila and Polcura Rivers (Figure 3a), a wedge-shaped plateau formed by late Pleistocene valley-confined lava covers folded strata of the Cura-Mallín Formation (Figure 6c). The plateau consists of ~1 km^3 of basaltic lavas that probably erupted during a single event because there are no interbedded slope deposits expected from the steep topographic gradient to the east. The plateau morphology, valley confinement, wedge shape, and alignment with the surface ruptures of the Quique River indicate that the ascension of these flows occurred along the LLFS. Two uneroded fault scarps probably of Holocene age cut the surface of the plateau bounding a small depression (Figure 6c).

[22] Immediately north of the Chillán volcano, two parallel approximately north-south to north-northeast oriented glacial valleys are located along the northward prolongation of the LLFS (Figure 2). The valleys run parallel to the axis of Tertiary folds and are probably controlled by basement faults. The eastern valley, which would correspond to the direct along-strike northward prolongation of the LLFS, is filled by a lava flow dated as 641 ± 20 ka (Ar-Ar/whole rock [*Dixon et al.*, 1999]). No field evidence of faults cutting either this lava or unconsolidated deposits was found in this area.

5.1.2. Seismic Reflection and Bathymetric Profiles

[23] Near the northern end of the lake, bathymetric profiles image several relatively small north-south oriented scarps, which increase in relief southward. Seismic profiles 28, 28-1, 35, and 35-1 image three main north-northwest striking faults that form a complex horst-and-graben structure with many secondary faults (inset map, Figure 3c; profile, Figure 6e). The faults seem to have an anastomosed pattern hard to follow along these four profiles, but the major graben-bounding fault can be well correlated to a continuous bathymetric break.

[24] The seismic and bathymetric profiles indicate that slip magnitude increase toward the center of the lake. Along the shore, recent slope debris and the strong variations in water level have eroded all the evidence of surface ruptures. Normal faults that control tilted hanging wall blocks are imaged in the north-south oriented profile 47, but as cross profiles are not available here, fault strikes are undefined and thus not confidently extended southward. Anyway, east-west bathymetric profiles show continuous breaks suggesting that faults are connected with the seismically imaged system farther south (Figure 3c).

[25] The highest fault scarps of this northern segment generate about 5.5 m of relief in the flat lake bottom. Assuming that the upper lacustrine drape cut by these faults is younger than 7.1 cal ka, the faults would have a minimum slip rate of 0.77 mm/yr, which is consistent with the rate determined for the faulted pyroclastics of the Polcura River (Figure 6d). However, the faults cut the lake bottom and thus their latest increment must be younger. Slip along this segment increase toward the center of the lake.

5.2. Central LLFS Segment

5.2.1. Surface Ruptures

[26] On the western shore of the central part of the lake, *Niemeyer and Muñoz* [1983] mapped several northeast striking normal faults that cut the Cura-Mallín Formation. These faults are prominent features on the aerial photo and cut a glaciated surface indicating recent activity (Figure 7a). Two normal faults juxtapose the Cola de Zorro and Cura-Mallín formations at the eastern shore of Lago Laja (Figure 3a). Here, the northeast striking Béjar fault converges with a west-northwest striking normal fault; both have about 300 m throw, but their prolongation into the lake is not imaged on the seismic data and thus their late Quaternary activity is uncertain.

5.2.2. Seismic Reflection and Bathymetric Profiles

[27] Seismic profile 04 is east-west oriented and located in the central part of the lake (Figure 3c). The center of this profile images two half graben structures with associated antithetic faults in the hanging wall and a central horst pillar.

Figure 6. Northern segment of the Lago Laja fault system. (a) Shaded relief DEM and map of Holocene rupture zones. (b) Air photo of the Quique valley. White triangles show Holocene ruptures. Note alignment of vegetation due to concentrated spring of water along the fractured fault zone. (c) Cross section showing a valley-confined basaltic plateau erupted along the main fault. (d) Southward view of normal faults cutting Holocene fallout pyroclastic deposits from the Chillán volcano. These deposits are correlated with the intermediate age group of *Dixon et al.* [1999], which range from 6.5 to 6.1 cal ka. (e) Normal faults imaged by reflection seismic profile Laja 35. For location see Figure 6a and inset on Figure 3c. Note the similarity between the fault geometry in this profile and the outcrop in Figure 6d.

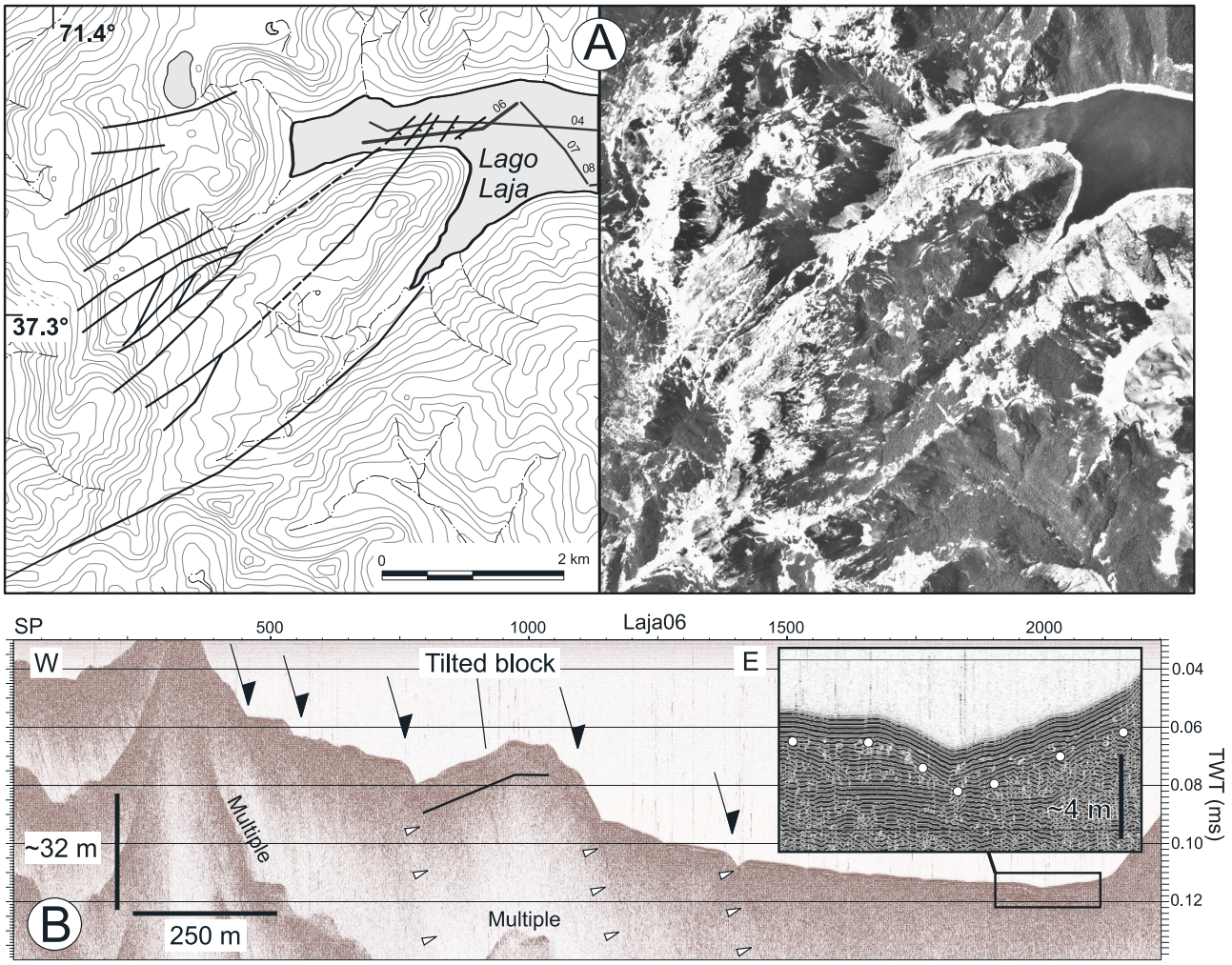

Figure 7. Western part of the central Lago Laja fault system segment. (a) Topographic map and aerial photo of the Machos Bay area showing fresh surface ruptures. These faults cut a glacially polished surface on Tertiary rocks, and their extension into the lake is correlated with subaqueous faults imaged by seismic profiles Laja 06 and 04. (b) Reflection seismic profile Laja 06 showing the subaqueous expression of the faults interpreted from the aerial photo. Inset shows the erosional unconformity and the upper lacustrine drape.

The eastern half graben is shown in Figure 8. Profile 06 is east-west oriented, located in the western sector of the Machos Bay (Figure 3c) and images three east-down normal faults. The eastern at shotpoint (SP) 750 tilted a hanging wall block; the fault at SP 1100 generates an about 12-m-high scarp formed by two steps that cut the tilted block (Figure 7b). These faults have a northeast strike as correlated with profile 04, a parallel line immediately north, and are interpreted as the extension of the northeast striking onshore normal faults observed in the aerial photo (Figure 7a). The fresh fault traces are consistent with the Holocene activity determined from the seismic profiles.

[28] In the eastern part of profile 06, the high-resolution 3.5 kHz data images a paleochannel that truncates subhorizontal sediments and produced about 3.5 m of incision. Subsequently, ~1.8 to 2 m of well-bedded sediments corresponding to the uppermost lacustrine drape downlap against the erosional surface and cover the paleorelief formed by channel incision (inset, Figure 7b). This erosional unconformity is related to the opening of the lake's dam during the Antuco 1 collapse event at 7.1 ± 0.09 cal ka. This implies that the fault at SP 1100 that offsets this horizon by 12 m has a minimum slip rate of 1.7 mm/yr, which is significantly higher than rates along the northern segment.

5.3. Southern LLFS Segment

5.3.1. Surface Ruptures

[29] South of Lago Laja, along the Campamento River (Figure 3), Holocene fallout pyroclastic deposits from the nearby Antuco volcano and unconsolidated fluvial conglomerates are locally cut by east-west striking subvertical normal faults, which have 50 to 80 cm of slip. In contrast to

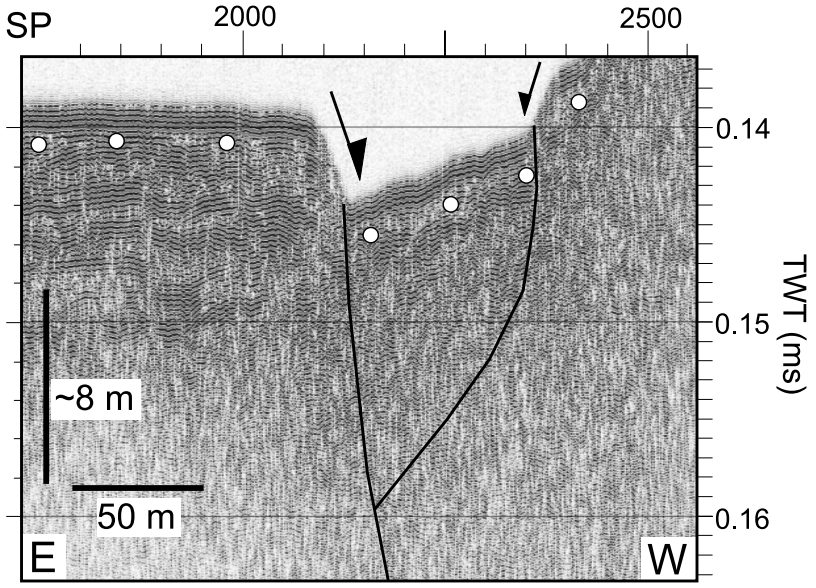

Figure 8. Central Lago Laja fault system. Extract of reflection seismic profile Laja 04 shows a hemigraben structure with an antithetic fault in the center of the lake. For location, see Figure 3c. The white dots indicate the 7.1 ka erosional unconformity.

the faults of the other segments, the structures here are not clearly related to a topographic break in the landscape and are only observed in incised fluvial terraces. Slip magnitude is much lower in this area, and no evidence of Quaternary normal faults were found farther south along the Trapa-Trapa River.

5.3.2. Seismic Reflection and Bathymetric Profiles

[30] Immediately north of the Antuco volcano in the widest part of the lake, a ~2-km-long, north-south striking scarp is observed in three east-west oriented parallel bathymetric profiles (Figure 3c). Seismic profile 01 crosses this scarp and images an east dipping normal fault that cuts the uppermost sediments. Because of the proximity of the Antuco volcano, the sediments are imaged as less continuous and slightly undulated reflecting input of volcanoclastic material. This east facing scarp is up to 19 m high and thus the causative normal fault would have a minimum vertical slip rate of 2.6 mm/yr on its southern part.

5.3.3. Structure of the Antuco and Cóndor Volcanoes

[31] Mount Cóndor is an eroded Pleistocene volcanic center located on the western flank of the Antuco volcano (Figure 9). A dike swarm is exposed on the glaciated flat top surface of this center. The dikes have a mean azimuth of 039 ± 5° (1σ SD; n = 16). If these dikes are Andersonian as has been proposed for northeast oriented neotectonic volcanic conduits along the Patagonian Andes [*Nakamura*, 1977; *López-Escobar et al.*, 1995; *Lara et al.*, 2004], their orientation should be parallel to the axis of maximum horizontal stress (SH_{max}) [*Anderson*, 1951]. The Antuco's active summit crater and three vents located on the southwestern flank also form a northeast oriented alignment (Figure 9), which should also be parallel to SH_{max} [*Nakamura*, 1977]. Two other vents are emplaced along the rim of the Antuco 1 collapse caldera. The Herradura minor eruptive center is located near the lake's shore on the northeastern base of the Antuco, and is probably related to the fault imaged immediately north (Figure 9).

6. Soft-Sediment Deformation Structures Adjacent to the LLFS: Paleoseismic Significance

[32] Southeast of Lago Laja along the Pinos River (Figure 3), fluvial incision exposed a sequence of glaciolacustrine sediments. The paleolake covered ~10 km^2 and its surface was above 1400 m asl, at least 50 m higher than the maximum level of the present lake (Figure 10a). This paleolake was probably not connected to the modern Laja basin, as no similar lacustrine deposits were found in its surroundings and both areas are separated by a ridge formed by Tertiary bedrock (Figures 3a and 10a). Subsequent incision of the ridge by the Pinos River connected this region to the present Laja basin.

[33] The lacustrine sequence consists of clay, fine ash, occasionally fine to medium sand with pumice clasts, and rarely fine conglomerate (Figure 10b). The sequence has a minimum thickness of 20 m, its base is not exposed and the top is an erosional surface covered by colluvial and pyroclastic deposits. The lack of organic material and the presence of drop stones (Figure 10f) indicate deposition during a glacial period, probably in a proglacial lake formed during the ice retreat phase. Because the preservation potential of soft sediments deposited during old glacial periods is very low [*Gibbons et al.*, 1984], these lacustrine sediments presumably date from the last glaciation, whose end is well dated at ~10 ka in the 40°S region [*Lowell et al.*, 1995]. Judging from the distribution of frontal moraines and

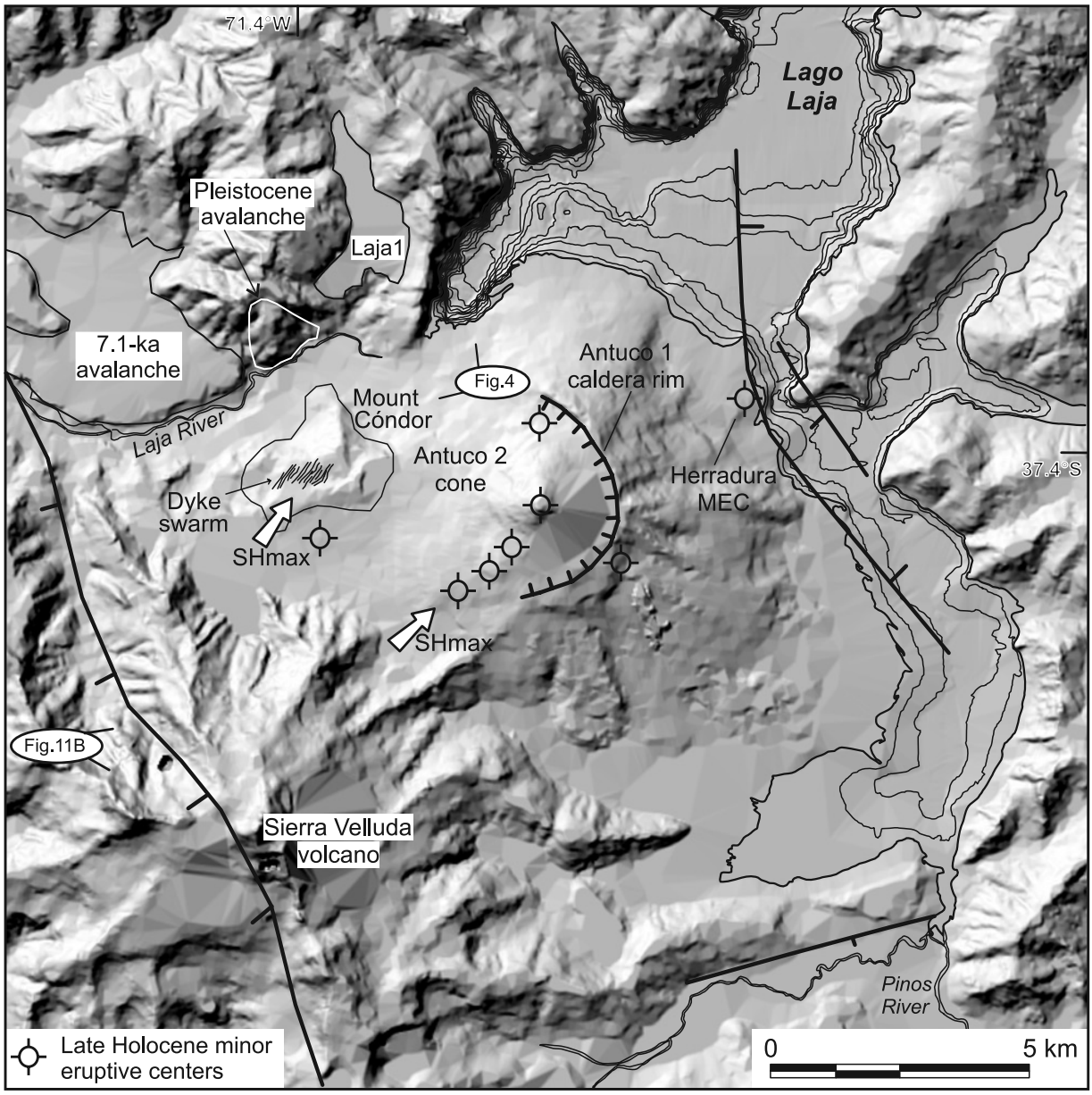

Figure 9. Shaded relief DEM and map of the Antuco volcano area illustrating the distribution of late Quaternary minor eruption centers, recent faults, and volcanotectonic features discussed in the text.

previous glacial reconstructions [*Laugenie*, 1982], the whole Lago Laja area was covered by glaciers during the Last Glacial Maximum (LGM) at ~19 ka. Thus the lacustrine sediments should postdate the LGM but predate the end of the last glaciation at ~10 ka.

[34] In the northern part of the paleolake, east-northeast striking normal faults with centimeter-scale offsets cut the lacustrine deposits. Generally, these sediments are horizontal, but on the flank of the bedrock ridge they are tilted 15°N and unconformably covered by horizontal conglomerates. A steep east-northeast oriented topographic break separates the tilted beds from similar horizontal layers, which crop out 25 m below. This scarp is parallel to the tilted beds and extends westward for at least 5 km into the Petronquines River. We relate it to a south-southeast dipping normal fault (Figure 10a). In the footwall ridge, a small depression filled with fluvial conglomerates overlays the lacustrine sediments. This saddle-like depression, which hosts the international road to Pichachén Pass, is interpreted as the result of fluvial erosion by a former tributary of Lago Laja, which was then abandoned due to normal faulting and footwall uplift forming a wind gap (Figure 10a).

[35] Layers affected by soft-sediment deformation are present in the lacustrine sequence. The deformed beds range from 10 cm to 2.4 m in thickness. The deformation structures are centimeter- to meter-scale tight isoclinal, asymmetric, and

overturned folds, with linear wavy geometries and locally pillow-like structures (Figures 10c and 10e). A layer of medium-grained sand is present at the base of all but one of the deformed beds (BSD in Figures 10d and 10e).

[36] The deformed soft-sediment layers meet the six field criteria for their relation to "seismites" and paleoearthquakes proposed among others by *Sims* [1975], *Hempton and Dewey* [1983], *Obermeier* [1996], and *Bowman et al.* [2004] (Table 1):

[37] 1. Clay-rich sediments are not the most susceptible to liquefaction because of their cohesion, but almost all of the deformed beds have a basal layer of fine to medium sand. This basal water-saturated porous sand is confined by the less permeable overlying clay. During an earthquake, the sand layer would loose cohesion, liquefy and act as a detachment for the overlying clay that would deform plastically.

[38] 2. Three beds with similar deformation structures are exposed in the thicker section (Figure 10b).

[39] 3. The fine laminated clay suggests still water lacustrine conditions and the lack of rotational slips or displaced material typical of slumps, decreases the possibility of slope control as a cause for soft-sediment deformation. Moreover, the friable laminated sediments are expected to be pulverized during turbulent transport.

[40] 4. A sandwiched position is observed in all the deformed horizons. Clear rhythmic alternation of deformed and undisturbed layers may also indicate the instantaneous nature of seismic triggering, implying that deformation occurred shortly after deposition [*Jones and Omoto*, 2000].

[41] 5. From a total of 10 outcrops of lacustrine sediments, nine have deformed layers and in the tenth the sediments are cut by normal faults.

[42] 6. The linear wavy geometry shown in Figure 10e is very similar to the seismites described in the Dead Sea Basin by *Heifetz et al.* [2005], which have been precisely dated and correlated to historical earthquakes [*Migowski et al.*, 2004]. Thus we interpret the soft-sediment deformation structures as seismites, and relate them to earthquakes nucleated along the LLFS during the late Pleistocene. The >2-m-thick seismites and existence of surface ruptures indicates that the LLFS is capable of generating M>6 events [*Allen*, 1982; *Wells and Coppersmith*, 1994].

7. Quaternary Extensional Structures in the Laja Region

[43] Since the end of intra-arc orogenic shortening at ~5 Ma, extensional and transtensional tectonics have dominated the intra-arc region between ~36 and 39°S [*Folguera et al.*, 2002, 2003; *Melnick et al.*, 2006a]. Northeast of Lago Laja, the north-northeast striking Béjar fault juxtaposes Oligo-Miocene sediments of the Cura-Mallín Formation with Pliocene–early Pleistocene volcanic rocks from the Cola de Zorro Formation (Figure 3a). This steep fault has at least 350 m of down-to-east throw and has a clear topographic expression extending for ~18 km (Figure 3b). The Cola de Zorro Formation is continuously exposed from this area to the eastern foothills of the Main Cordillera in Argentina, where it has an age range of 4.0 to 1.2 Ma (K-Ar/whole rock [*Folguera et al.*, 2004; *Miranda et al.*, 2006]). West of the Béjar fault, the Toro graben is an elongated 3×1.7 km^2, northeast oriented tectonic depression that hangs over the upper Polcura River (Figure 3a). The two graben-bounding normal faults offset the angular unconformity between the Cura-Mallín and Cola de Zorro formations by 300 m vertically. On the western part of the graben, a zone of hydrothermal alteration is localized along the steep northern fault. The southern fault, on the other hand, is well exposed at a roadcut along the upper Polcura River where it dips 80° NW. Both the Toro and Béjar faults have vertical slip rates of ~0.1–0.2 mm/yr. However, no clear evidences of Holocene activity were observed along these faults.

[44] Deep glacial erosion exposed the interior of the Sierra Velluda volcano, which consists of two units: the lower unit, dated as 495 ± 88 ka, is formed by ~1500 m of lavas and breccias with interbedded pyroclastic flows; and the upper unit dated as 381 ± 40 ka is formed mainly by ~1000 m of lavas and breccias (K-Ar/whole rock [*Moreno et al.*, 1985]). On the northwestern slope of the volcano, a northwest striking southwest dipping normal fault cuts a 2000-m-high section of the volcano with 500 ± 50 m throw (Figure 11a). This fault juxtaposes the upper and lower units of the volcano truncating the pyroclastic flows of the lower sequence (Figure 11b), and has a vertical slip rate of 1.3 ± 0.3 mm/yr. As no caldera collapse events have been described nor identified in the current survey for this Pleistocene volcano, we relate this fault to extensional tectonics.

8. Deformation Rates of the Lago Laja Fault System

[45] Slip rates have been calculated for the faulted pyroclastic deposits and subaqueous faults of the northern and central LLFS, respectively, which have age-constrained stratigraphic markers. Because the time seismic sections do

Figure 10. Soft-sediment deformation structures. (a) Map showing outcrops of late Pleistocene glaciolacustrine sediments, estimated extent of the former lake, and recent normal faults. The 20-m topographic contours derived from the photogrammetric restitution of 1:70,000 aerial photos (photos were taken in 1998, a dry year when the border of the lake was lower than in Figure 3). (b) Stratigraphic column of the late Pleistocene glaciolacustrine sequence. (c) Thickest soft-sediment deformation structures interpreted as seismite. Note that it is sandwiched by horizontal lying undeformed beds. (d) A sandwiched seismite with a layer of sand at its base. During lateral compression caused by seismic waves, this water-saturated porous layer, which is confined by the less permeable overlying clay, would liquefy and acted as a basal detachment (BSD) allowing the clay beds to deform plastically. (e) Pillow-like deformed bed with sand blows injected into the axial plane of the anticline. (f) Drop stone in lacustrine sediments.

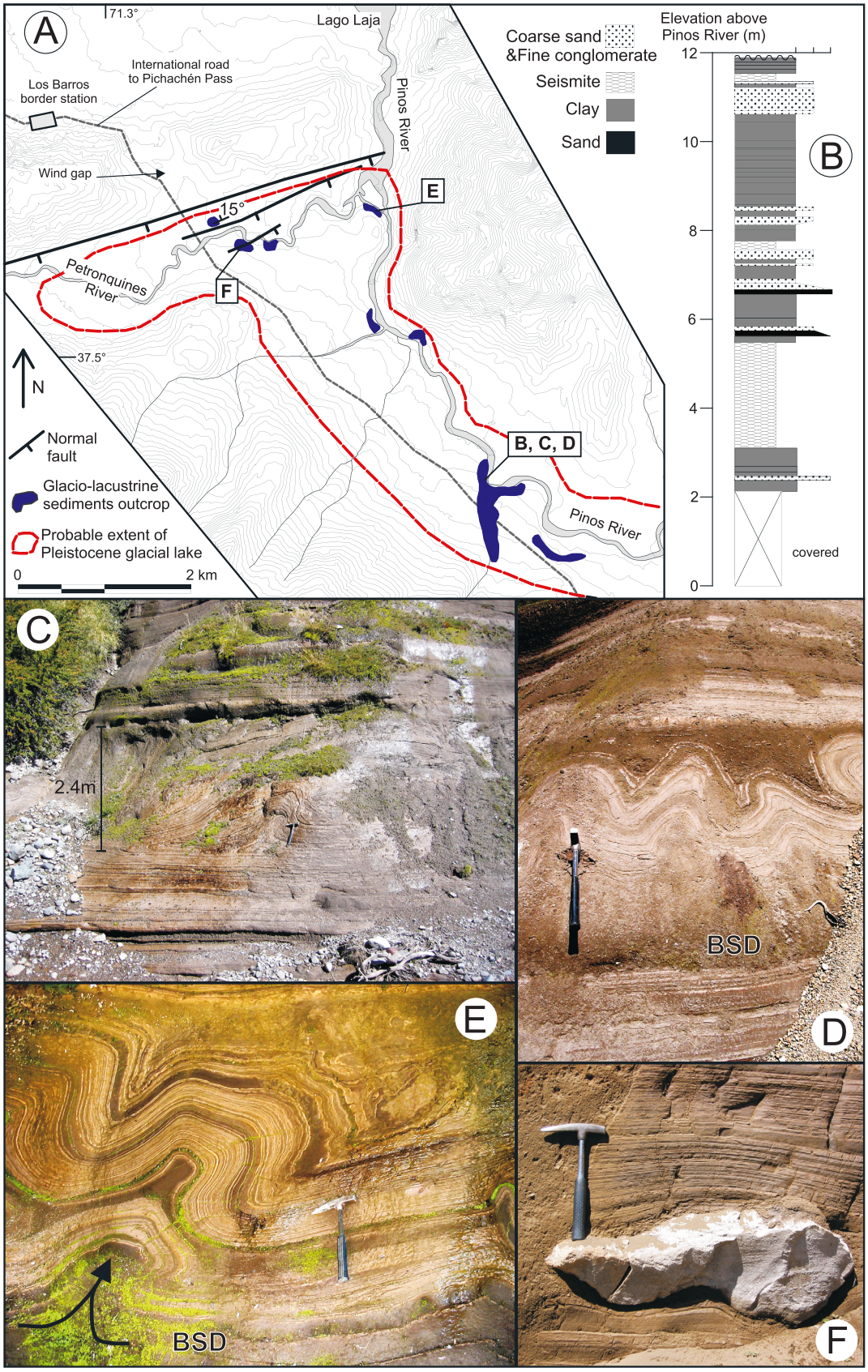
A
71.3°
Lago Laja
International road
to Pichachén Pass
Los Barros
border station
Pinos River
Wind gap
15°
E
F
Petronquines
River
37.5°
N
Normal
fault
Glacio-lacustrine
sediments outcrop
Probable extent of
Pleistocene glacial lake
0
2 km
B, C, D
Pinos River
Coarse sand
&Fine conglomerate
Seismite
Clay
Sand
Elevation above
Pinos River (m)
12
10
8
6
4
2
0
B
covered
C
2.4m
BSD
D
E
BSD
F

Figure 10

Table 1. Field Criteria for the Relation of Soft-Sediment Structures to Seismites[a]

No.	Field Criteria for the Identification of Seismites
1	suitable sediments, loosely consolidated
2	cyclic repetitions of similar structures
3	preclusion of trigger by gravity flows or slope instabilities
4	a stratigraphically sandwiched position
5	lateral continuity and regional abundance
6	similarity to structures reported elsewhere or formed in experiments under earthquake-induced shaking

[a]Proposed among others by *Sims* [1975], *Hempton and Dewey* [1983], *Obermeier* [1996], and *Bowman et al.* [2004].

not allow estimating true inclinations, a 10° error is assigned to the dips of the subaqueous faults, which range from 60 to 85°. This range estimate is consistent with the rather steep exposed Holocene faults (Figure 6d). The fault parameters, slip rates, and seismic profiles used to derive these data are presented in Table 2, and fault group numbers are shown in Figure 3b. These rates should be considered as minimum because they are mostly based on the 7.1 ka age of the erosional unconformity, but most faults cut through this layer implying younger activity and thus faster rates. The average minimum east-west extension rate for the whole fault system is 1.2 ± 0.6 mm/yr (1σ SD), obtained by adding fault groups in latitudinal sections and averaging them (Table 2). The higher averaged rate of 2.0 ± 1.0 mm/yr occurs in the central and deepest part of the lake. Total post-7.1 ka east-west extension is about 0.7% and the average strain rate is in the order of 3×10^{-14} s^{-1}.

[46] The Holocene extension rate is about an order of magnitude higher than the rates estimated for the Pliocene–early Pleistocene Toro and Béjar faults (<0.1 mm/yr) and still about twice the rate of the mid-Pleistocene Sierra Velluda fault (~0.7 mm/yr). Even if these estimates are limited, they indicate an acceleration over the Quaternary.

9. Quaternary Shortening Along the Foothills of the Main Cordillera

9.1. Eastern Foothills: Copahue-Antiñir Fault System

[47] The Copahue-Antiñir Fault System (CAFS) (Figures 1 and 2) extends for over 110 km along the Argentinean back-arc region from 37.8°S northward, and represents the southernmost expression of the active central Andean orogenic front. This system consists of east vergent reverse faults and folds that affect 4.0 to 1.2 Ma plateau lavas from the Cola de Zorro Formation (K-Ar/whole rock [*Folguera et al.*, 2004; *Miranda et al.*, 2006]), Pleistocene conglomerates, and lacustrine sediments [*Iaffa et al.*, 2002; *Melnick et al.*, 2002]. Dextral offsets of ephemeral streams and a lava flow are well exposed along the southern sector of the CAFS leading *Folguera et al.* [2004] to interpret the whole fault system as transpressional. In the southern sector a 3.1 ± 0.2 Ma lava flow is dextrally displaced 195 m, yielding a low strike-slip rate of 0.06 mm/yr (K-Ar/whole rock [*Folguera et al.*, 2004]). However, there is no clear evidence of dextral deformation along the central and northern sectors of this fault system. The CAFS has a marked concave-to-the-west trace (Figure 2) and higher shortening magnitude occurred in its central sector. Therefore the subordinated right-lateral deformation in the southern sector is likely an effect of the concave trace and accommodation of the along-strike gradient in shortening, rather than bulk transpression.

[48] Along the Reñilelvú section, which represents the central sector of the CAFS, about 0.5–0.8 km of shortening have occurred since 1.2 ± 0.1 Ma at an average shortening rate of 0.5 ± 0.2 mm/yr. In this sector deformation has occurred along a 13-km-wide zone accounting thus for ~5% of shortening and an average east-west strain rate in the order of -10^{-14} s^{-1}. The strain rate of the northern and southern sectors should be similar as deformation occurs along a narrower area and shortening magnitudes are lower.

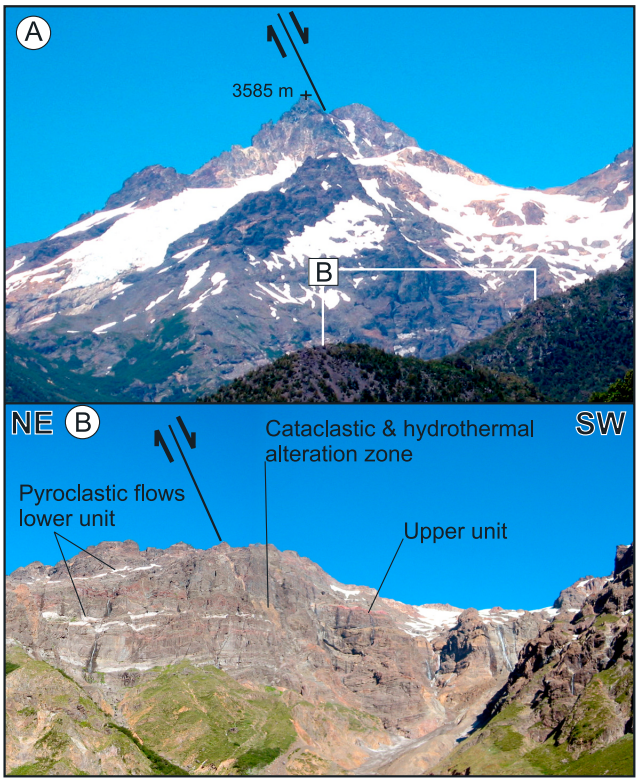

Figure 11. (a) View to the southeast of the Sierra Velluda volcano from the intermediate Laja valley. Note the trace of the southwest dipping normal fault that cuts a 2500-m-high section of the volcano with ~500 m throw. (b) Detailed view of the fault at the upper Malalcura valley (see Figure 9 for location). The fault juxtaposes the upper and lower units of the volcano truncating the pyroclastic flows from the inferior unit. A 15-m-wide cataclastic zone overprinted by hydrothermal alteration fills the fault zone. Normal drag is observed in the hanging wall beds.

Table 2. Holocene Slip Rates of the Lago Laja Fault System[a]

	Age of Faulted Unit, calibrated ka	Seismic Profiles Used	Number of Faults	Fault Parameters					Vertical		Horizontal		E-W	
				Throw,[b] m	± Error[c]	Dip, deg	± Error[d]	Azimuth, deg	Slip Rate,[e] mm/yr	± Error	Slip Rate, mm/yr	± Error	Slip Rate mm/yr	± Error
Pyroclastics	6.1–6.5		6	6.5	0.1	75	2	5	1.03	0.05	0.28	0.04	0.28	0.04
Group 1	<7.1	1,57	2	18.5	1.9	70	10	0	2.59	0.29	0.94	0.49	0.94	0.49
Group 2	<7.1	2,14	3	20.5	2.1	70	10	65	2.87	0.32	1.05	0.54	0.44	0.23
Group 3	<7.1	3,4	5	42.5	4.3	70	10	35	5.95	0.66	2.17	1.12	1.78	0.91
Group 4	<7.1	4,9,3	5	23	2.3	80	10	355	3.22	0.36	0.57	0.57	0.57	0.57
Group 5	<7.1	11,12,48,50	6	40	4.0	70	10	0	5.60	0.62	2.04	1.05	2.04	1.05
Group 6	<7.1	28,35,39,43	9	22	2.2	80	10	355	3.08	0.34	0.55	0.54	0.54	0.54
Average[f]									0.68	0.37	1.90	0.74	1.24	0.63

[a]Subaqueous fault group numbers and location of seismic lines shown in Figure 3c. Horizontal averages for groups in latitudinal sections: 1 + 2, 3 + 4, 5, and 6 (1σ errors).
[b]Cummulative throw for all faults in the respective group.
[c]We assume 10% error in measurements from seismic lines.
[d]Since our seismic lines are not depth converted, we assume 10° error in dip estimates.
[e]Minimum cumulative vertical slip rate for all faults in the respective group.
[f]Vertical rate average per fault.

9.2. Western Foothills: Huépil Fault

[49] Near Huépil, the piedmont of the Main Cordillera is deformed by a ~10-km-wide, north-northeast striking anticline and cut by a parallel reverse fault (Figures 2 and 12). This piedmont surface is formed by alluvial breccias, pyroclastic flows, and fluvial conglomerates of the Malleco Formation [*Suárez and Emparán*, 1997]. The age of this unit is bracketed by several 4.4 ± 0.5 to 0.8 ± 0.3 Ma lava flows interbedded near the base and top of the predominantly fluvial-alluvial sequence, respectively (K-Ar/whole rock [*Suárez and Emparán*, 1997]). Thus the folded surface near Huépil should be younger than 0.8 ± 0.3 Ma.

[50] Immediately west of Tucapel, alluvial beds of the Malleco Formation strike north-south and dip 15°E (Figure 12). This eastward inclination is opposite to the usual dip direction of the Malleco beds, which follow the westward inclined depositional slope. These folded beds conform the eastern flank of a small range, which we interpret as an asymmetric anticline. The Laja River cuts the anticline forming a gorge; on its walls two ~50-m-thick polygenic sequences are exposed with a marked contact surface, which is smoothly folded parallel to the depositional surface. Several small internally drained basins formed in the crestal region of the northern anticline, and are probably related to continuous channel slope decrease due to uplift and abandonment from the Laja drainage. The Huépil anticline has a maximum relief of 130 m from the present Laja River bed, so assuming an age of 0.8 ± 0.3 Ma for the upper part of the Malleco Formation yields a minimum growth rate of 0.18 ± 0.07 mm/yr for the central part of the anticline. This is a conservative estimate since the upper surface is probably younger and the Laja River bed is filled with recent terraces that have decreased relief.

[51] On the western flank of the fold, a north-northeast striking, west facing scarp cuts the Malleco beds generating about 30 m of relief. This scarp is interpreted to be caused by an east dipping Quaternary reverse or thrust fault to which the anticline is related. Northward, the fault continues along the Cholguán River where two marked west facing scarps control the development of range-parallel drainages (Figure 12). Late Miocene west vergent reverse faults and fault-related folds have been widely described along the western edge and foothills of the Main Cordillera between 33 and 38°S [e.g., *Godoy et al.*, 1999; *Melnick et al.*, 2006a; *Servicio Nacional de Geología y Minería*, 2003]. We interpret the Huépil fault as the neotectonic expression of such a structure. More Quaternary contractional structures probably exist along the western foothills, but the lack of good exposures due to low relief and extensive vegetation has made their identification difficult. Crustal microearthquakes registered by the ISSA local network [*Bohm et al.*, 2002] occur below the western foothills (Figure 13) and are probably related to the Huépil contractional structure.

10. Discussion

10.1. Tectonic Interpretation of Intra-arc Extensional Deformation

[52] Our observations suggest regionally limited Quaternary extensional deformation along the axis of the intra-arc. The LLFS extent (36.9–37.6°S) is coincident with the Copahue-Antiñir contractional system located ~40 km east along the Andean foothills (Figure 2). Folding and faulting of Quaternary sediments also occurs at this latitude along the western piedmont of the Main Cordillera (Figure 12). In consequence, Quaternary shortening concentrates along its foothills forming a large-scale pop-up structure, while coeval extension is localized along its axial, volcanically active, and topographically highest zone (Figure 13). The strain rates of the LLFS and back-arc reverse fault system are of the same magnitude ($\sim 10^{-14}$ s^{-1}).

[53] One plausible interpretation for the synorogenic extension along the LLFS is incipient gravitational collapse of the Main Cordillera's core. Limited collapse, which extracts potential energy from the thickened crust is

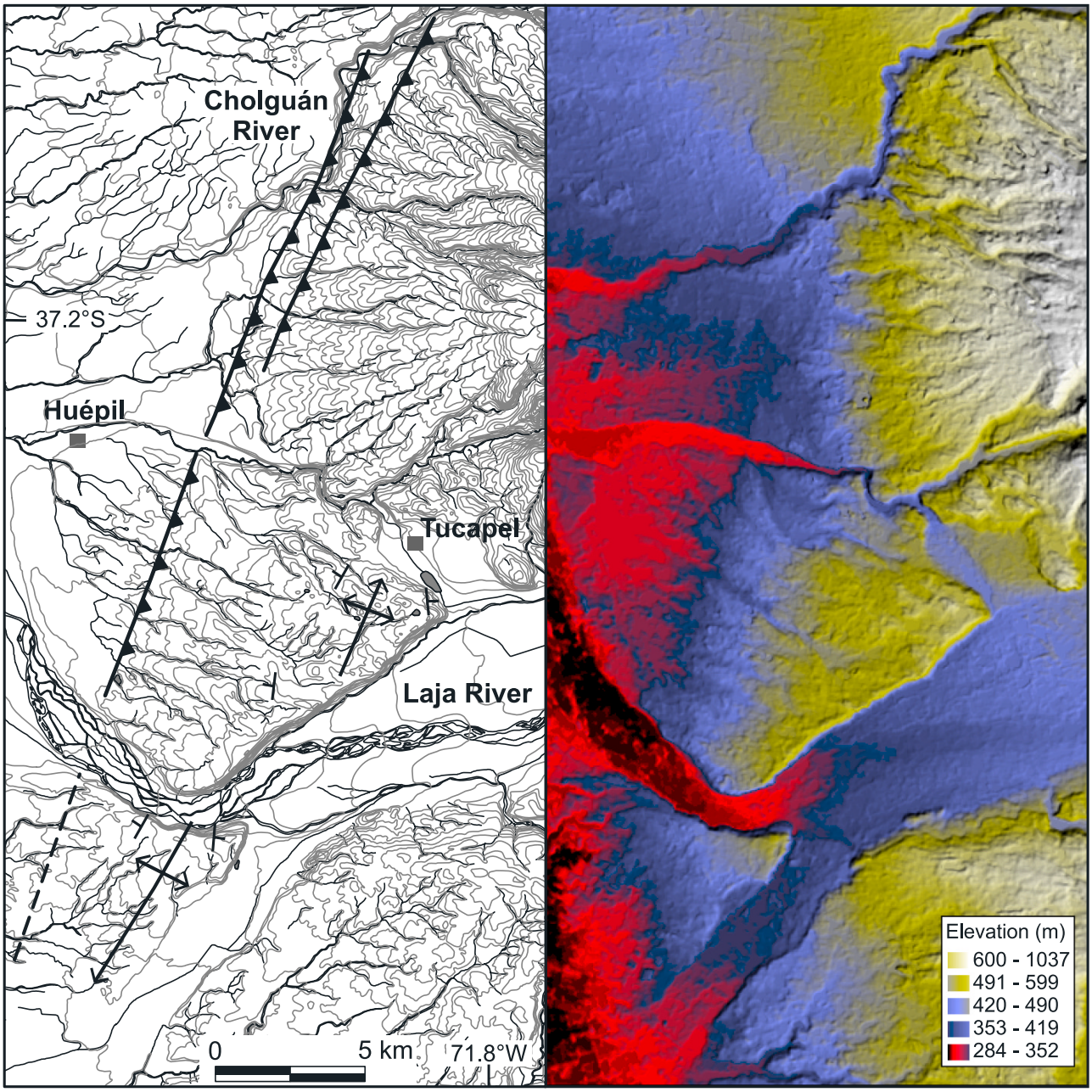

Figure 12. Map of the Huépil contractional structures along the western foothills of the Main Cordillera. See Figure 2 for location. (right) Shaded relief DEM (15-m horizontal resolution) derived from ASTER (Advanced Spaceborne Thermal Emission and Reflection Radiometer) satellite imagery. (left) Structural map, 25-m topographic contours, and drainage network.

induced by ongoing crustal shortening [e.g., *Molnar and Lyon-Caen*, 1988; *Buck and Sokoutis*, 1994; *Liu et al.*, 2000]. This phenomenon, coeval shortening and extension, has been described along the Andes in Perú [e.g., *Dalmayrac and Molnar*, 1981] and the Altiplano-Puna plateau [e.g., *Allmendinger et al.*, 1997], as well as in other mountain belts in the world [e.g., *Mercier et al.*, 1987; *Echtler and Malavieille*, 1990; *Selverstone*, 2005]. The Laja Andes are rather triangular in cross section and thrusting occurs along both foothills; so, considering modeling by *Royden* [1996], its collapse implies the absence of an intracrustal low-viscosity layer and coupling between the crust and motion of the mantle. In fact, no crustal discontinuity has been imaged by receiver function [*Yuan et al.*, 2006] and tomography surveys [*Bohm et al.*, 2002] in the Laja region, while similar data imaged a large midcrustal low-viscosity layer across the flat-topped Altiplano plateau [*Yuan et al.*, 2000].

[54] The elevated heat flow along the volcanic arc most likely contributed to a rheological weakening of structures in the Lago Laja region, facilitating and localizing deformation. It is also plausible that synorogenic extension is enhanced by cooling of intrusions below the arc. As most of this area was completely covered by glaciers during the Quaternary ice ages, postglacial lithospheric rebound and unbending have probably also contributed to uplift causing subsequent isostatic compensation of surface loads during the Holocene (see below). Lower crustal flow in this region has probably not contributed significantly to synorogenic extension [e.g., *Bird*, 1991], because here the lower crust should consist of high viscosity restites produced by ~150 Myr of stationary arc magmatism [*Mpodozis and Ramos*, 1989; *Tassara and Yáñez*, 2003].

10.2. Transient Unloading and Localization of Faulting

[55] *Bevis et al.* [2004] showed that the vertical component of the continuous GPS record from the ANTC site, located 20 km west of Lago Laja (Figure 2), is experiencing nonsteady fluctuations with a range of 50 mm since 1997. They found that these variations are very well correlated with changes in Lago Laja's volume due to the seasonal hydropower management, and thus the fluctuations of the GPS data are dominated by the Earth's local elastic response to the changing weight of water. *Hetzel and Hampel* [2005] modeled the extensional deformation of the Wasatch region showing that lithospheric rebound caused by fast unloading, in this case by postglacial emptying of Lake Boneville, led to an increase in slip rates and localized deformation. Thereon this is a reasonable explanation for the paleoearthquake clustering and slip acceleration observed during the last ~10 kyr in the Wasatch region. A parameter study of this process showed that loading magnitude mostly controls the slip rate increase after unloading [*Hampel and Hetzel*, 2006].

[56] The Holocene faults of the LLFS that have the largest displacements and slip rates are in the central, deepest part of the lake. Here, slip rates are at least three times higher than along the shallow northern part as well as onshore sectors of the fault system (Table 2). These observations raise the question as whether the Holocene unloading episode caused by deglaciation and the outburst megaflood event at 7.1 ka enhanced fault activity in the deeper part of Lago Laja, where loading magnitudes were higher and which should be rebounding faster.

10.3. Lago Laja Fault System and Strain Partitioning Along the Margin

[57] Along the Patagonian Andes (38–46°S), most of the margin-parallel component of oblique plate convergence has been accommodated along the intra-arc region by the Liquiñe-Ofqui strike-slip fault zone, and thus a high degree of strain partitioning occurs [*Dewey and Lamb*, 1992; *Lavenu and Cembrano*, 1999; *Rosenau et al.*, 2006]. This is supported by the oblique orientation of SH_{max} along the volcanic arc, fault kinematic and regional structural data, and focal mechanisms. The northernmost geomorphic evidence of Holocene dextral strike-slip deformation along the volcanic arc come from the Lonquimay Valley (38.5°S) and Copahue area (38°S) [*Melnick et al.*, 2006a].

[58] In contrast, no geomorphic evidence for strike-slip deformation was found along the LLFS in the field and in the detailed examination of stereo aerial photos. A strike-slip component may be inferred from (1) some of the seismically imaged fault arrays in the center of the lake, which suggest negative flower structures (Figure 5); (2) the general fault pattern of the LLFS conformed by a main north-south striking branch and several northeast striking subsidiary faults; and (3) the prominent northeast strike of the dikes at Mount Cóndor and the aligned flank vents of the Antuco volcano both suggesting a northeast orientation of SH_{max} (Figure 9). However, if some margin-parallel dextral shear has occurred along the LLFS, it must have been of much lower magnitude than the rate of geomorphic decay of the landscape and thus not observable in the field, in contrast to the structures south of 38°S. This raises the question as to how oblique convergence is partitioned at 37°S. Probably very minor dextral shear has occurred diffusely along the arc but surely much less than south of 38°S.

[59] In order to visualize and understand the major along-strike kinematic variations between the central and Patagonian Andes, we integrate the fore-arc structures. At this latitude, the fore arc is divided in two kinematic domains limited by the Arauco Peninsula (Figures 1 and 13). In the southern domain oblique shortening occurs along northwest striking faults with a left-lateral component, while along the northern domain oblique shortening occurs along northeast striking faults, which in turn have a right-lateral component. This fore-arc kinematic boundary across Arauco is spatially coincident with the intra-arc kinematic boundary over the Callaqui-Copahue-Mandolegüe transfer zone (CCM in Figure 13), which decouples the discrete Liquiñe-Ofqui strike-slip system from the LLFS and Copahue-Antiñir dip-slip systems [*Melnick et al.*, 2006a]. These observations emphasize that north of Arauco and Copahue (37.5–38°S) a higher magnitude of the margin-parallel component of oblique subduction has been accommodated in the coastal region due to the favorable fault orientations, while in turn to the south a higher magnitude has been accommodated by dextral strike-slip faulting along the intra-arc region. This segment boundary, named Arauco transition zone, marks the change from the low and narrow Patagonian Andes to the high and broad central Andes, and a steep gradient in the degree of strain partitioning. North of the Arauco transition the margin-parallel shear induced by oblique convergence is absorbed along a wide zone with small amounts of diffuse strike-slip deformation, while to the south strain is partitioned into the discrete Liquiñe-Ofqui strike-slip fault zone. The Arauco Peninsula is the largest deflection of the coastline along the Pacific of South America, and like other peninsulas of the Andean margin (i.e., Pisco, 14°S; Mejillones, 23°S; and Taitao, 46.5°S peninsulas [e.g., *Mpodozis and Ramos*, 1989]), is related to a major along-strike change in deformation style, subduction earthquake ruptures, tectonic evolution, and topography of the entire orogen.

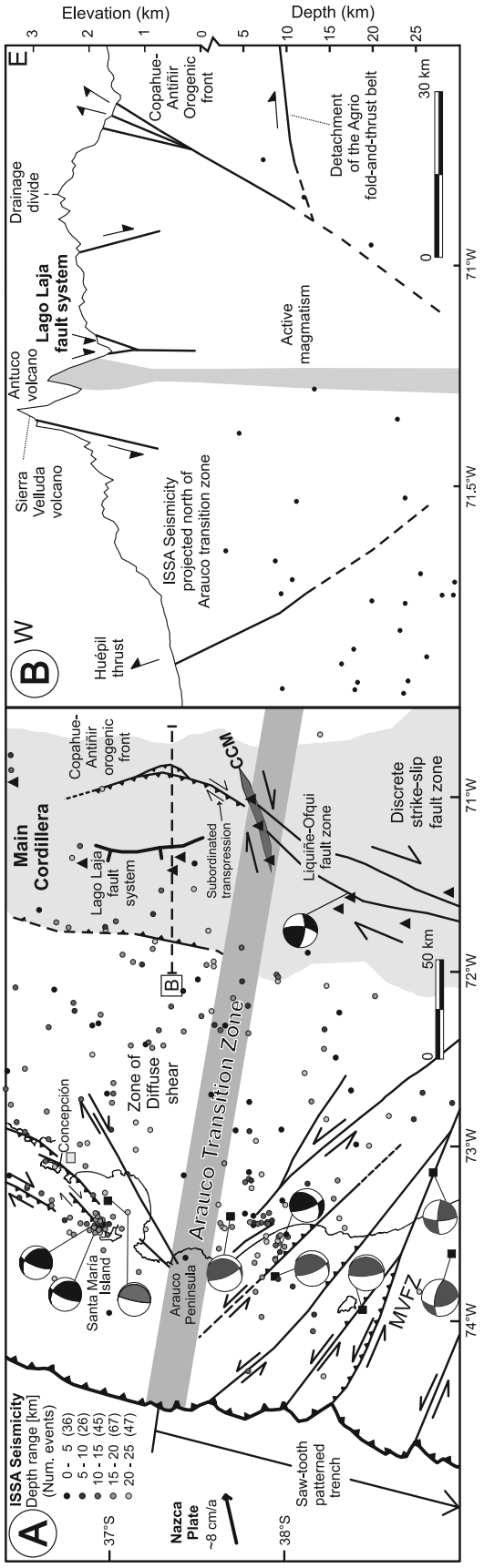

10.4. Seismic Hazards Posed by the Lago Laja Fault System

[60] Although the Laja region is mostly uninhabited, earthquakes here pose a regional hazard. Surface ruptures along the northern active faults could damage the two hydrocarbon pipelines along the upper Polcura River. The seiche waves caused by an earthquake nucleated in one of the subaqueous faults of the lake could damage the hydroelectric power stations, which are the major hydropower suppliers in Chile. In any case, the highest hazard is posed by the eventual rupture of the narrow dam of Lago Laja by tectonic and/or volcanic activity, retaining 4.7 km^3 of water. The opening of the dam would trigger an outburst megaflood as has happened at least twice before, latest at 7.1 ka,

Figure 13. (a) Neotectonic map of the Andean margin illustrating the kinematic changes across the Arauco transition zone, which integrates the Arauco Peninsula in the fore arc and Callaqui-Copahue-Mandolegüe (CCM) transfer zone in the intra-arc. Two contrasting kinematic domains are differentiated across this segment boundary: (1) the southern domain, which in the fore arc is dominated by oblique shortening along northwest striking faults that have a left-lateral component controlling the saw-tooth pattern of the trench (interpreted from multibeam bathymetry collected by *Reichert and the SPOC Team* [2002]); the major fault is the Mocha-Villarica fault zone (MVFZ) [*Melnick et al.*, 2003]; and in the intra-arc of this southern domain, dextral strike-slip deformation occurs along the Liquiñe-Ofqui fault zone (LOFZ); and (2) the northern domain in turn is characterized by oblique shortening along northeast striking reverse faults with right-lateral component in the fore arc, and in the intra-arc by shortening along the Copahue-Antiñir fault system in the eastern foothills of the Main Cordillera and locally along its western piedmont region as well, while extension occurs along the Lago Laja fault system in the axial region. The Arauco transition zone marks a northward decreasing gradient in the degree of strain partitioning, as deduced from the distribution of margin-parallel shear in a broad zone to the north and in the discrete Liquiñe-Ofqui fault zone to the south and the boundary between the central and Patagonian Andes. Depth-coded crustal seismicity is from the ISSA local network [*Bohm et al.*, 2002]; number of events is given in parentheses. Black focal mechanisms in the fore arc are from *Bruhn* [2003], and those in the arc are from *Barrientos and Acevedo-Aranguiz* [1992]. Gray focal mechanisms from the NEIC and USGS catalogues. Fore-arc structures interpreted from ENAP-Chile industry reflection seismic profiles [*Melnick et al.*, 2006b; *Melnick and Echtler*, 2006]. (b) Maximum topography over a 30-km-wide swath of the Main Cordillera illustrating the active structures. See Figure 13a for location. Seismicity projected from the region north of the Arauco transition zone. Agrio fold-and-thrust belt detachment extrapolated from seismic reflection profiles acquired immediately east in the Neuquén Basin [*Zapata and Folguera*, 2005].

presenting a severe risk to many settlements in the Central Depression and along the Bío-Bío River including Concepción, the second largest city of Chile.

11. Conclusions

[61] Field observations, interpretation of reflection seismic profiles, aerial photos, and combined bathymetric-topographic DEMs indicate late Pleistocene-Holocene extensional faulting along the Andean intra-arc zone at ~37°S. The deformation pattern defines the Lago Laja fault system, which has an average minimum east-west Holocene extensional rate of 1.2 mm/yr. Soft-sediment deformation structures in late Pleistocene glaciolacustrine deposits are interpreted as seismites and related to M>6 paleoearthquakes. No strike-slip component in the deformation has been recorded in geomorphic markers.

[62] Extensional deformation occurs along the axial, higher region of the Main Cordillera, and is coeval and spatially related to two contractional systems. These systems are located along the eastern and western foothills and have opposite vergence defining a large-scale pop-up structure responsible for uplift of the Main Cordillera. In this context, we interpret extension in terms of incipient gravitational collapse of the highest part of the Andes in response to crustal thickening in a thermally weakened volcanic domain. Extension is over imposed to the isostatic compensation of surface loads caused by postglacial rebound, which could have led to the observed acceleration of the deformation during the latest Quaternary.

[63] The lack of strike-slip deformation expected from oblique convergence at 37°S contrasts with the dextral fault zone that extends continuously south of 38°S along the Patagonian Andes volcanic arc. We interpret this kinematic change along the volcanic arc to be caused by a first-order seismotectonic segment boundary, the Arauco transition zone, located at the Arauco Peninsula in the fore arc (37.5°S). Favorable fault orientations north of Arauco accommodate oblique shortening absorbing and distributing the margin-parallel component of plate convergence in the fore arc. The structures in the Laja region result from regional tectonic changes along the orogen, underlining the necessity of integrating regional and local observations to gain insight into processes responsible for seismotectonic segmentation of convergent margins.

[64] **Acknowledgments.** This work was supported by International Quality Network (IQN) project at University of Potsdam founded by the German Academic Exchange Found (DAAD), GeoForschungsZentrum Potsdam Southern Andes Project, and Collaborative Research Center SFB 267 "Deformation Processes in the Andes" founded by the German Science Foundation (DFG). The seismic data were collected in the framework of the Belgian OSTC project EV/12/10B "A continuous Holocene record of ENSO variability in southern Chile" and with the support in the field of K. De Rycker, E. Chapron, and R. Brümmer and M. Pino at Universidad Austral de Chile (Valdivia) and W. San Martín and R. Urrutia of EULA at the Universidad of Concepción. D.M. is grateful to O. Oncken and M. Strecker for their continuous support. This work benefits from discussions with A. Folguera, M. Rosenau, A. Tassara, V.A. Ramos, E. Godoy, and B. Bookhagen. We thank K. Bataille and G. Hermosilla (University of Concepción), E. Bartulovic (Oleoducto Transandino S.A.), R. Verdugo (CONAF), and the staff of "Avanzada Cuatro Juntas" for logistical support and to R. Fuenzalida, H. Muñoz, and M. Sanchez for assistance during fieldwork. B. Scharf and O. Buettner (UFZ Leipzig-Halle) kindly shared their bathymetry of Lago Laja, acquired within the Chilean-German cooperation project "Water Resources and Energy: Aquatic ecosystem responses to water level" (WTZ 00/002), EULA supported their field work. C. Garzione, an anonymous reviewer, and Associate Editor C. Andronicos provided constructive comments.

References

Allen, J. R. L. (1982), *Sedimentary Structures: Their Character and Physical Basis*, 663 pp., Elsevier, New York.

Allmendinger, R. W., T. E. Jordan, S. M. Kay, and B. L. Isacks (1997), The evolution of the Altiplano-Puna plateau of the central Andes, *Annu. Rev. Earth Planet. Sci.*, *25*, 139–174.

Anderson, E. M. (1951), *The Dynamics of Faulting*, 191 pp., Oliver and Boyd, White Plains, N. Y.

Avé Lallemant, H. G., and J. S. Oldow (2000), Active displacement partitioning and arc-parallel extension of the Aleutian volcanic arc based on Global Positioning System geodesy and kinematic analysis, *Geology*, *28*, 739–742.

Barrientos, S. E., and P. S. Acevedo-Aranguiz (1992), Seismological aspects of the 1988–1989 Lonquimay (Chile) volcanic eruption, *J. Volcanol. Geotherm. Res.*, *53*, 73–87.

Barrientos, S., E. Vera, P. Alvarado, and T. Monfret (2004), Crustal seismicity in central Chile, *J.S. Am. Earth Sci.*, *16*, 759–768, doi:10.1016/j.jsames.2003.12.001.

Bertrand, S., X. Boes, J. Castiaux, F. Charlet, R. Urrutia, C. Espinoza, G. Lepoint, B. Charlier, and N. Fagel (2005), Temporal evolution of sediment supply in Lago Puyehue (southern Chile) during the last 600 yr and its climatic significance, *Quat. Res.*, *64*, 163–175, doi:10.1016/j.yqres.2005.06.005.

Bevis, M., E. Kendrick, A. Cser, and R. Smalley Jr (2004), Geodetic measurement of the local elastic response to the changing mass of water in Lago Laja, Chile, *Phys. Earth Planet. Inter.*, *141*, 71–78, doi:10.1016/j.pepi.2003.05.001.

Bird, P. (1991), Lateral extrusion of lower crust from under high topography, in the isostatic limit, *J. Geophys. Res.*, *96*, 10,275–10,286.

Bohm, M., S. Lüth, H. Echtler, G. Asch, K. Bataille, C. Bruhn, A. Rietbrock, and P. Wigger (2002), The southern Andes between 36°S and 40°S latitude: Seismicity and average velocities, *Tectonophysics*, *356*, 275–289.

Bowman, D., A. Korjenkov, and N. Porat (2004), Late-Pleistocene seismites from Lake Issyk-Kul, the Tien Shan range, Kyrghyzstan, *Sediment. Geol.*, *163*, 211–228, doi:10.1016/S0037-0738(03)00194-5.

Brüggen, J. (1941), El volcán Antuco y la geología glacial del valle del Laja, *Rev. Chilena Hist. Geogr.*, *91*, 356–385.

Bruhn, C. (2003), Momententensoren hochfrequenter Ereignisse in Sudchile, Ph.D. thesis, 181 pp., Univ. of Potsdam, Potsdam, Germany.

Buck, W. R., and D. Sokoutis (1994), Analogue model of gravitational collapse and surface extension during continental convergence, *Nature*, *369*, 737–740.

Cembrano, J., F. Hervé, and A. Lavenu (1996), The Liquiñe Ofqui fault zone: A long-lived intra-arc fault system in southern Chile, *Tectonophysics*, *259*, 55–66.

Chapron, E., C. Beck, M. Pourchet, and J. F. Deconinck (1999), 1822 earthquake-triggered homogenite in Lake Le Bourget (NW Alps), *Terra Nova*, *11*, 86–92.

Charlet, F., C. Marchand, S. Volland, M. Pino, R. Urrutia, J. Müller, E. Chapron, and M. De Batist (2003), Reflection-seismic study of six lakes in south-central Chile (37°S–42°S): Lagos Laja, Lleulleu, Icalma, Villarrica, Puyehue & Todos Los Santos, paper presented at X Congreso Geológico Chileno, Univ. de Concepción, Concepción, Chile.

Chinn, D. S., and B. L. Isacks (1983), Accurate source depths and focal mechanisms of shallow earthquakes in western South America and in the New Hebrides island arc, *Tectonics*, *2*, 529–563.

Dalmayrac, D., and P. Molnar (1981), Parallel thrust and normal faulting in Peru and constraints on the state of stress, *Earth Planet. Sci. Lett.*, *55*, 473–481.

Delpino, D., and M. Deza (1995), Mapa geológico de la provincia de Neuquén, Republica Argentina, scale 1:500,000, Serv. Geol. y Minero Argent., Buenos Aires.

Dewey, J. F., and S. H. Lamb (1992), Active tectonics of the Andes, *Tectonophysics*, *205*, 79–95.

Dixon, H. J., M. D. Murphy, S. J. Sparks, R. Chavez, J. A. Naranjo, P. N. Dunkley, S. R. Young, J. S. Gilbert, and M. R. Pringle (1999), The geology of Nevados de Chillán volcano, Chile,, *Rev. Geol. Chile*, *26*, 227–253.

Domeyko, I. (1846), Memoria sobre la Estructura Geológica de Chile en la Latitud de Concepción, desde la Bahía de Talcahuano hasta la Cumbre de la Cordillera de Pichachén y descripción del Volcán Antuco, in *Geología*, vol. 5, edited by I. Domeyko pp. 123–172, Imprenta Cervantes, Santiago.

Echtler, H., and J. Malavieille (1990), Extensional tectonics, basement uplift and Stephano-Permian collapse basin in a late Variscan metamorphic core complex (Montagne Noire, southern Massif Central), *Tectonophysics*, *177*, 125–138.

Eyles, N., B. Koseoglu, J.I. Boyce, and J. D. Halfman (2000), Seismic stratigraphy of Waterton Lake, a sediment-starved glaciated basin in the Rocky Mountains of Alberta, Canada and Montana, USA, *Sediment. Geol.*, *130*, 283–311.

Fitch, T. J. (1972), Plate convergence, transcurrent faults, and internal deformation adjacent to southeast Asia and the western Pacific, *J. Geophys. Res.*, *77*, 4432–4460.

Folguera, A., V. A. Ramos, and D. Melnick (2002), Transición de los Andes Patagónicos a los Andes Centrales: Extremo norte del sistema de Liquiñe-Ofqui (38°S), *Rev. Geol. Chile*, *29*, 227–240.

Folguera, A., V. A. Ramos, and D. Melnick (2003), Recurrencia en el desarrollo de cuencas de intraarco Cordillera Neuquina (37°30′–38°S), *Rev. Asoc. Geol. Argent.*, *58*, 3–19.

Folguera, A., V. A. Ramos, R. L. Hermanns, and J. Naranjo (2004), Neotectonics in the foothills of the southernmost central Andes (37°–38°S): Evidence of strike-slip displacement along the Antiñir-Copahue fault zone, *Tectonics*, *23*, TC5008, doi:10.1029/2003TC001533.

Giacosa, R. E., and C. N. Heredia (2004), Structure of the north Patagonian thick-skinned fold-and-thrust belt, southern central Andes, Argentina (41°–42°S), *J. S. Am. Earth Sci.*, *18*, 61–72.

Gibbons, A., J. Megeath, and K. Pierce (1984), Probability of moraine survival in a succession of glacial advances, *Geology*, *12*, 327–330.

Godoy, E., G. Yañez, and E. Vera (1999), Inversion of an Oligocene volcano-tectonic basin and uplifting of its superimposed Miocene magmatic arc in the Chilean central Andes: First seismic and gravity evidences, *Tectonophysics*, *306*, 217–236.

Hampel, A., and R. Hetzel (2006), Response of normal faults to glacial-interglacial fluctuations of ice and water masses on Earth's surface, *J. Geophys. Res.*, *111*, B06406, doi:10.1029/2005JB004124.

Heifetz, E., A. Agnon, and S. Marco (2005), Soft sediment deformation by Kelvin Helmholtz instability: A case from Dead Sea earthquakes, *Earth Planet. Sci. Lett.*, *236*, 497–504.

Hempton, M. R., and J. F. Dewey (1983), Earthquake-induced deformational structures in young lacustrine sediments, East Anatolian Fault, southeast Turkey, *Tectonophysics*, *98*, 7–14.

Hetzel, R., and A. Hampel (2005), Slip rate variations on normal faults during glacial-interglacial changes in surface loads, *Nature*, *435*, 81–84, doi:10.1038/nature03562.

Hughen, K., C. Herring, O. Marchal, S. Lehman, J. Turnbull, J. Southon, and J. Overpeck (2004), ^{14}C Activity and global carbon cycle changes over the past 50,000 years, *Science*, *303*, 202–207, doi:10.1126/science.1090300.

Iaffa, D., E. González Díaz, and A. Folguera (2002), Tectónica postglaciaria en la Cordillera Neuquina: Río Picunleo (37°30′S), paper presented at XV Congreso Geológico Argentino, Asoc. Geol. Argent., El Calafate.

Jarrard, R. D. (1986), Relations among subduction parameters, *Rev. Geophys.*, *24*, 217–284.

Jones, A. P., and K. Omoto (2000), Towards establishing criteria for identifying trigger mechanisms for soft-sediment deformation: A case study of late Pleistocene lacustrine sands and clays, Onikobe and Nakayamadaira basins, northeastern Japan, *Sedimentology*, *47*, 1211–1226.

Jordan, T. E., B. L. Isacks, R. W. Allmendinger, J. A. Brewer, V. A. Ramos, and C. J. Ando (1983), Andean tectonics related to geometry of subducted Nazca plate, *Geol. Soc. Am. Bull.*, *94*, 341–361.

Jordan, T. E., W. Matthew Burns, R. Veiga, F. Pángaro, P. Copeland, S. Kelley, and C. Mpodozis (2001), Extension and basin formation in the southern Andes caused by increased convergence rate: A mid-Cenozoic trigger for the Andes, *Tectonics*, *20*, 308–324.

Kemnitz, H., W. Kramer, and M. Rosenau (2005), Jurassic of Tertiary tectonic, volcanic, and sedimentary evolution of the southern Andean intra-arc zone, Chile (38–39°S): A survey, *Neues Jahrb. Geol. Palaontol.*, *236*, 19–42.

Kendrick, E., M. Bevis, R. Smalley Jr., B. Brooks, R. C. Vargas, E. Lauría, and L. P .S. Fortes (2003), The Nazca–South America Euler vector and its rate of change, *J.S. Am. Earth Sci.*, *16*, 125–131, doi:10.1016/S0895-9811 (03)00028-2.

Kley, J., C. R. Monaldi, and J. A. Salfity (1999), Along-strike segmentation of the Andean foreland: Causes and consequences, *Tectonophysics*, *301*, 75–94.

Lara, L. E., J. A. Naranjo, and H. Moreno (2004), Rhyodacitic fissure eruption in southern Andes (Cordón Caulle; 40.5°S) after the 1960 (M_w:9.5) Chilean earthquake: A structural interpretation, *J. Volcanol. Geotherm. Res.*, *138*, 127–138, doi:10.1016/j.jvolgeores.2004.06.009.

Laugenie, C. (1982), La Région des Lacs, Chili Meridional, Recherches sur l'Evolution Geomorphologique d'Un Piemont Glaciaire Quaternaire Andin, Ph.D. thesis, 822 pp., Univ. de Bordeaux III, Talence, France.

Lavenu, A., and J. Cembrano (1999), Compressional- and transpressional-stress pattern for Pliocene and Quaternary brittle deformation in fore arc and intra-arc zones (Andes of central and southern Chile), *J. Struct. Geol.*, *21*, 1669–1691.

Liu, M., Y. Shen, and Y. Yang (2000), Gravitational collapse of orogenic crust: A preliminary three-dimensional finite element study, *J. Geophys. Res.*, *105*, 3159–3173.

Lohmar, S. (2000), Estratigrafía, Petrografía y Geoquímica del Volcán Antuco y sus depósitos (Andes del Sur, 37°25′S), M. S. thesis, 115 pp., Univ. de Concepción, Concepción, Chile.

Lomnitz, C. (2004), Major earthquakes of Chile: A historical survey, 1535–1960, *Seismol. Res. Lett.*, *75*, 368–378.

Lowell, T. V., C. J. Heusser, B. G. Andersen, P. I. Moreno, A. Hauser, L. E. Heusser, C. Schlüchter, D. R. Marchant, and G. H. Denton (1995), Interhemispheric correlation of late Pleistocene glacial events, *Science*, *269*, 1541–1549.

López-Escobar, L., J. Cembrano, and H. Moreno (1995), Geochemistry and tectonics of the Chilean southern Andes basaltic Quaternary volcanism (37–46°S), *Rev. Geol. Chile*, *22*, 219–234.

Lüth, S., et al. (2003), A crustal model along 39°S from a seismic refraction profile-ISSA 2000, *Rev. Geol. Chile*, *30*, 83–94.

Melnick, D., and H. P. Echtler (2006), Inversion of forearc basins in south-central Chile caused by rapid glacial age trench fill, *Geology*, *34*, 709–712, doi:10.1130/G22440.1.

Melnick, D., A. Folguera, M. Rosenau, H. Echtler, and S. Potent (2002), Tectonics from the northern segment of the Liquiñe-Ofqui fault system (37°–39°s), Patagonian Andes, paper presented at Fifth International Symposium of Andean Geodynamics, Inst. de Rech. pour le Dév., Toulouse, France.

Melnick, D., M. Sanchez, H. Echtler, and V. Pineda (2003), Structural geology of Mocha Island, south-central Chile (38°30′S, 74°W): Regional tectonic implications, paper presented at X Congreso Geológico Chileno, Univ. de Concepción, Concepción, Chile.

Melnick, D., M. Rosenau, A. Folguera, and H. Echtler (2006a), Neogene tectonic evolution of the Neuquén Andes western flank (37–39°S), in *Evolution of an Andean Margin: A Tectonic and Magmatic View From the Andes to the Neuquén Basin (35°–39°S lat)*, edited by S. M. Kay, and V. A. Ramos *Spec. Pap. Geol. Soc. Am.*, *407*, 73–95, doi:10.1130/2006.2407 (04).

Melnick, D., B. Bookhagen, H.P. Echtler, and M.R. Strecker (2006b), Coastal deformation and great subduction earthquakes, Isla Santa María, Chile (37°S), *Geol. Soc. Am. Bull.*, *118*, 1463–1480, doi:10.1130/B25865.1.

Mercier, J. L., R. Armijo, P. Tapponnier, E. Carey-Gailhardis, and H. Tong Lin (1987), Change from late Tertiary compression to Quaternary extension in southern Tibet during the India-Asia collision, *Tectonics*, *6*, 275–304.

Migowski, C., A. Agnon, R. Bookman, J. F. W. Negendank, and M. Stein (2004), Recurrence pattern of Holocene earthquakes along the Dead Sea transform revealed by varve-counting and radiocarbon dating of lacustrine sediments, *Earth Planet. Sci. Lett.*, *222*, 301–314, doi:10.1016/j.epsl.2004.02.015.

Miranda, F., A. Folguera, P. R. Leal, J. A. Naranjo, and A. Pesce (2006), Upper Pliocene to lower Pleistocene volcanic complexes and late Neogene deformation in the south central Andes (36°30′–38°S), in *Evolution of an Andean Margin: A Tectonic and Magmatic View From the Andes to the Neuquén Basin (35°–39°S lat)*, edited by S. M. Kay, and V. A. Ramos, *Spec. Pap. Geol. Soc. Am.*, *407*, 287–298, doi:10.1130/2006.2407 (13).

Molnar, P. (1988), Continental tectonics in the aftermath of plate tectonics, *Nature*, *335*, 131–137.

Molnar, P. and H. Lyon-Caen (1988), Some simple physical aspects of the support, structure, and evolution of mountain belts, in *Processes in Continental Lithospheric Deformation*, edited by B. C. Clark, J. Burchfiel, and J. Suppe, *Spec. Pap. Geol. Soc. Am.*, *218*, 179–207.

Moreno, H., R. Thiele, A. Lahsen, J. Varela, L. López-Escobar, and M. Vergara (1985), Geocronología de Rocas Volcánicas Cuaternarias en los Andes del Sur entre las latitudes 37° y 38°S, Chile, *Rev. Asoc. Geol. Argent.*, *40*, 297–299.

Moreno, H., S. Lohmar, L. López-Escobar, and M. E. Petit-Breuilh (2000), Contribución a la evolución geológica, geoquímica e impacto ambiental del Volcán Antuco (Andes del Sur, 37°25′S), paper presented at IX Congreso Geológico Chileno, Soc. Geol. de Chile, Santiago.

Mpodozis, C., and V. Ramos (1989), The Andes of Chile and Argentina, in *Geology of the Andes and Its Relation to Hydrocarbon and Mineral Resources*, edited by G. E. Ericksen, M. T. Cañas Pinochet, and J. A. Reinemund pp. 59–90, Circum-Pac. Counc. for Energy and Miner. Resour., Houston, Tex.

Nakamura, K. (1977), Volcanoes as possible indicators of tectonic stress orientation - Principle and proposal, *J. Volcanol. Geotherm. Res.*, *2*, 1–16.

Niemeyer, H., and J. Muñoz (1983), Geología de la hoja Laguna de La Laja, map, scale 1:250,000, Serv. Nac. de Geol. y Miner., Santiago, Chile.

Obermeier, S. F. (1996), Using liquefaction-induced features for paleoseismic analysis, *Paleoseismology*, 331–396.

Petit-Breuilh, M. E. (1994), Actividad volcánica y cronología eruptiva histórica del volcán Antuco (37°24′S–71°22′W), Chile, *Rev. Geogr. Chile Terra Aust.*, *39*, 79–102.

Ramos, V. A. (1999), Plate tectonic setting of the Andean Cordillera, *Episodes*, *22*, 183–190.

Reichert, C. and the SPOC Team, (2002), Cruise report SO-161 Leg 2 and 3 SPOC: Subduction processes off Chile BMBF-Forschungsvorhaben 03G0161A, 154 pp., Bundesanst. für Geowiss. und Rohstoffe, Hannover, Germany.

Rosenau, M., D. Melnick, and H. Echtler (2006), Kinematic constraints on intra-arc shear and strain partitioning in the Southern Andes between 38°S and 42°S latitude, *Tectonics*, *25*, TC4013, doi:10.1029/2005TC001943.

Royden, L. (1996), Coupling and decoupling of crust and mantle in convergent orogens: Implications for strain partitioning in the crust, *J. Geophys. Res.*, *101*, 17,679–17,705.

Schnellmann, M., F. S. Anselmetti, D. Giardini, J. A. McKenzie, and S. N. Ward (2002), Prehistoric earthquake history revealed by lacustrine slump deposits, *Geology*, *30*, 1131–1134.

Selverstone, J. (2005), Are the Alps collapsing?, *Annu. Rev. Earth Planet. Sci.*, *33*, 113–132.

Servicio Nacional de Geología y Minería, (2003), Geologic map of Chile digital version, map, scale 1:1,000,000, Santiago, Chile.

Siame, L. L., O. Bellier, M. Sébrier, and M. Araujo (2005), Deformation partitioning in flat subduction

setting: Case of the Andean foreland of western Argentina (28°S–33°S), *Tectonics*, *24*, TC5003, doi:10.1029/2005TC001787.

Sims, J. D. (1975), Determining earthquake recurrence intervals from deformational structures in young lacustrine sediments, *Tectonophysics*, *29*, 141–152.

Somoza, R. (1998), Updated Nazca (Farallon)–South America relative motions during the last 40 My: Implications for mountain building in the central Andean region, *J.S. Am. Earth Sci.*, *11*, 211–215.

Stuiver, M., P. J. Reimer, E. Bard, J. W. Beck, G. S. Burr, K. A. Hughen, B. Kromer, G. McCormac, J. Van Der Plicht, and M. Spurk (1998), INTCAL98 radiocarbon age calibration, 24,000–0 cal BP, *Radiocarbon*, *40*, 1041–1083.

Suárez, M., and C. Emparán (1997), Hoja Curacautín: Regiones de la Araucanía y del Bío- Bío, map, scale 1:250,000, Serv. Nac. de Geol. y Miner., Santiago, Chile.

Tassara, A., and G. Yáñez (2003), Relationship between elastic thickness and the tectonic segmentation of the Andean margin (15–47°S), *Rev. Geol. Chile*, *30*, 159–186.

Tassara, A., H. J. Götze, S. Schmidt, and R. Hackney (2006), Three-dimensional density model of the Nazca plate and the Andean continental margin, *J. Geophys. Res.*, doi:10.1029/2005JB003976, in press.

Tebbens, S. F., and S. C. Cande (1997), Southeast Pacific tectonic evolution from early Oligocene to present, *J. Geophys. Res.*, *102*, 12,061–12,084.

Teyssier, C., B. Tikoff, and M. Markley (1995), Oblique plate motion and continental tectonics, *Geology*, *23*, 447–450.

Thiele, R., H. Moreno, S. Elgueta, A. Lahsen, S. Rebolledo, and M. E. Petit-Breuilh (1998), Quaternary geological-geomorphological evolution of the uppermost course of the Río Laja Valley, *Rev. Geol. Chile*, *25*, 229–253.

Tikoff, B., and C. Teyssier (1994), Strain modeling of displacement-field partitioning in transpressional orogens, *J. Struct. Geol.*, *16*, 1575–1588.

Vergara, M., and Y. Katsui (1969), Contribución a la geología y petrología del volcán Antuco, Cordillera de los Andes, Chile central, *Publ. 35*, pp. 25–47, Dep. de Geol., Univ. de Chile, Santiago.

Vergara, M., and J. Muñoz (1982), La Formación Cola de Zorro en la Alta cordillera Andina Chilena (36°–39°S), sus características petrográficas y petrológicas: Una revisión, *Rev. Geol. Chile*, *17*, 31–46.

Wells, D. L., and K. J. Coppersmith (1994), New empirical relationships among magnitude, rupture length, rupture width, rupture area, and surface displacement, *Seismol. Soc. Am. Bull.*, *84*, 974–1002.

Yáñez, G., and J. Cembrano (2004), Role of viscous plate coupling in the late Tertiary Andean tectonics, *J. Geophys. Res.*, *109*, B02407, doi:10.1029/2003JB002494.

Yuan, X., et al. (2000), Subduction and collision processes in the central Andes constrained by converted seismic phases, *Nature*, *408*, 958–961, doi:10.1038/35050073.

Yuan, X., G. Asch, K. Bataille, G. Bock, M. Bohm, H. Echtler, R. Kind, O. Oncken, and I. Wolbern (2006), Deep seismic images of the southern Andes, in *Evolution of an Andean Margin: A Tectonic and Magmatic View From the Andes to the Neuquén Basin (35°–39°S lat)*, edited by S. M. Kay, and V. A. Ramos, *Spec. Pap. Geol. Soc. Am.*, *407*, 61–72, doi:10.1130/2006.2407 (03).

Zapata, T., and A. Folguera (2005), Tectonic evolution of the Andean fold and thrust belt of the southern Neuquén Basin, Argentina, in *The Neuquén Basin: A Case Study in Sequence: Stratigraphy and Basin Dynamics*, edited by G. D. Veiga, et al., *Geol. Soc. Spec. Publ.*, *252*, 37–56.

H. P. Echtler and D. Melnick, GeoForschungsZentrum Potsdam, Telegrafenberg, D-14473 Potsdam, Germany. (melnick@gfz-potsdam.de)

F. Charlet and M. De Batist, Renard Centre of Marine Geology, University of Ghent, B-9000 Ghent, Belgium.